Int J Earth Sci (Geol Rundsch) (2017) 106:2549–2573
DOI 10.1007/s00531-017-1446-0

ORIGINAL PAPER

Late Paleozoic low-angle southward-dipping thrust in the Züünharaa area, Mongolia: tectonic implications for the geological structures in the Sayan-Baikal and Hangai-Daur belts

Gantumur Onon[1] · **Kazuhiro Tsukada**[2]

Received: 13 April 2016 / Accepted: 5 January 2017 / Published online: 26 February 2017
© The Author(s) 2017. This article is published with open access at Springerlink.com

Abstract The Central Asian Orogenic Belt (CAOB) is key to understanding the Paleozoic–Mesozoic geodynamics of Eurasian continent. The geological structure of the Middle-to-Late Paleozoic rock units in the North Mongolia–West Transbaikal region is critical in revealing development process of CAOB. The region is largely comprised of rocks from the continental affinity and accretionary complexes which form the Sayan-Baikal (SB) and Hangai-Daur (HD) belts. This paper describes the lithology, stratigraphy, geological structure, and U-Pb age of the rocks in the Züünharaa area, which is located within the Haraa terrane of the HD belt in Mongolia. We identified a regional low-angle southward-dipping thrust in this area. The tectonic implication of the low-angle south-dipping thrust is discussed within the North Mongolia–West Transbaikal region. The study area exposes metamorphosed clastic rocks of the Haraa Group intruded by Ordovician–Silurian granitic rocks, Devonian felsic volcanic rocks of the Ulaan Öndör Formation, and Visean clastic rocks of the Örmögtei Formation in ascending order. The Haraa Group, granitic rock, and Ulaan Öndör Formation are cut by the low-angle southward-dipping thrust throughout this area. The rocks along the thrust are fractured to form cataclasite zone up to ~40 m wide. The thrust includes granite–rhyolite clast of ~450–420 Ma, and is unconformably covered by Visean Örmögtei Formation. Therefore, thrusting occurred after Ordovician–Silurian and before Visean. Late Paleozoic low-angle southward-dipping thrusts, similar to the present study, are widely distributed in the Haraa terrane of the Hangai-Daur belt and in terranes of the Sayan-Baikal belt. Whereas, the contemporaneous southeast-verging composite folds and northward-dipping thrusts are developed in the accretionary complexes, which are exposed at south of the Haraa terrane. These contrasting structures suggest a couple of "landward-verging" and "oceanward-verging" structures and may correspond to the "doubly vergent asymmetric structure" of Alpine-type compressional orogen.

Keywords CAOB · North Mongolia–West Transbaikal region · Hangai-Daur belt · Late Paleozoic · Doubly vergent asymmetric structure

Introduction

The Altaid Collage (e.g., Sengör et al. 1993; Sengör and Natal'in 1996) or the Central Asian Orogenic Belt (CAOB; e.g., Janh et al. 2000; Xiao et al. 2003; Windley et al. 2007) is one of the largest Paleo-Mesozoic orogenic belts in the world (Fig. 1a). The CAOB lies among the Siberian craton (SC), East European craton (EEC), North China platform (NCP), and Tarim block (TB) and includes continental fragments, low–high T/P metamorphic rocks, ophiolite, continental/oceanic volcanic arc rocks, and accretionary complexes (Petrov et al. 2014). Its geological structure is key to understand the Paleo-Mesozoic geodynamic processes of the Eurasian continent. Various tectonic models for formation of the CAOB were presented. For instance, three major ideas are: (1) the continuous subduction–accretion of oceanic material along a long-lasting arc (Sengör et al. 1993; Sengör and Natal'in 1996); (2) the reworked collision of continental fragments rifted from the

✉ Gantumur Onon
oonkood@gmail.com

1 Graduate School of Environmental Studies, Nagoya University, Nagoya 464-8601, Japan

2 Nagoya University Museum, Nagoya University, Nagoya 464-8601, Japan

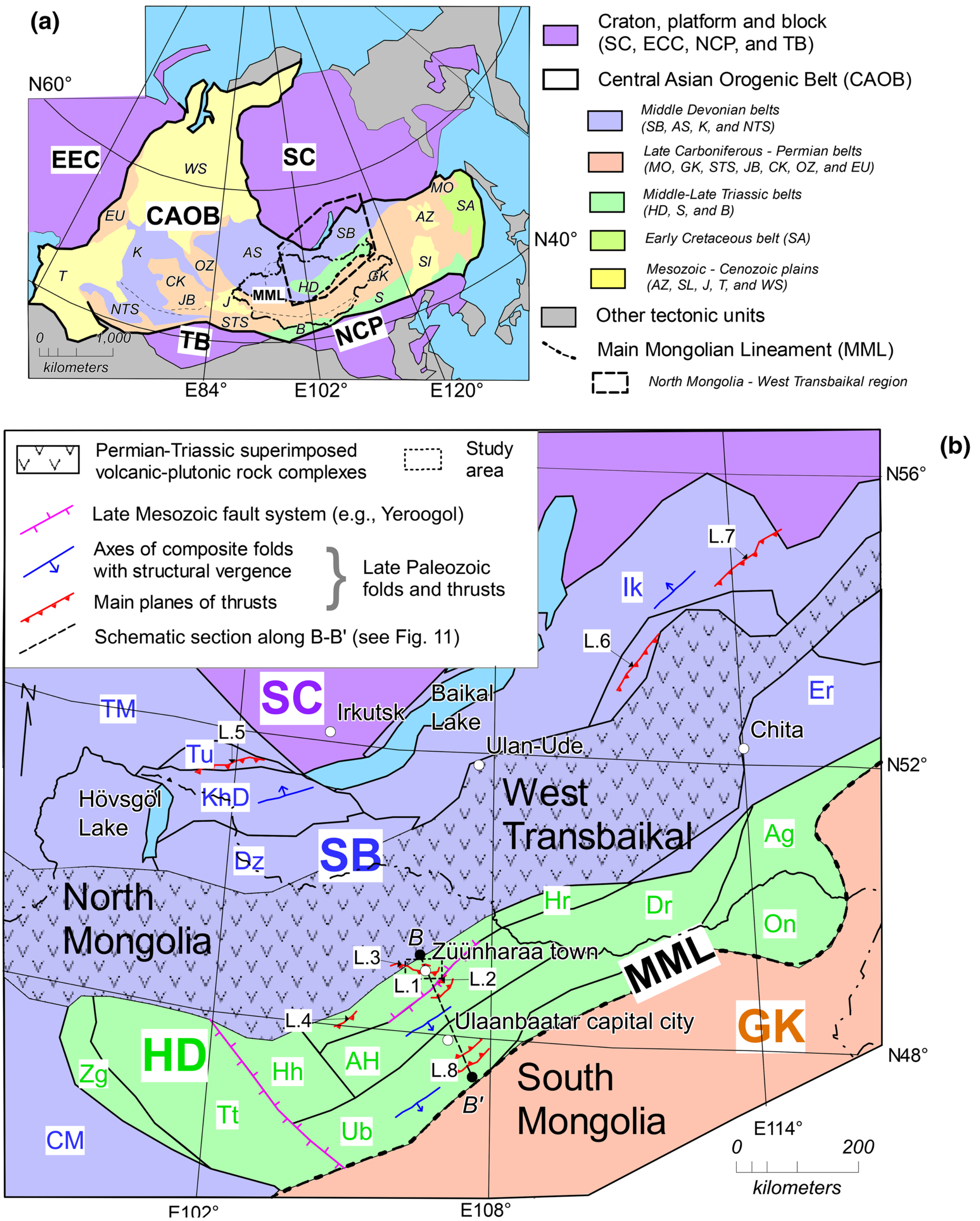
(a)
N60°
EEC
SC
WS
CAOB
EU
K
T
OZ
CK
JB
NTS
AS
SB
MML
HD
J
STS
GK
S
B
TB
NCP
MO
SA
AZ
SI
N40°
0
1,000
kilometers
E84°
E102°
E120°
Craton, platform and block (SC, ECC, NCP, and TB)
Central Asian Orogenic Belt (CAOB)
Middle Devonian belts (SB, AS, K, and NTS)
Late Carboniferous - Permian belts (MO, GK, STS, JB, CK, OZ, and EU)
Middle-Late Triassic belts (HD, S, and B)
Early Cretaceous belt (SA)
Mesozoic - Cenozoic plains (AZ, SL, J, T, and WS)
Other tectonic units
Main Mongolian Lineament (MML)
North Mongolia - West Transbaikal region
(b)
Permian-Triassic superimposed volcanic-plutonic rock complexes
Study area
Late Mesozoic fault system (e.g., Yeroogol)
Axes of composite folds with structural vergence
Main planes of thrusts
Late Paleozoic folds and thrusts
Schematic section along B-B' (see Fig. 11)
N56°
L.7
Ik
L.6
Er
N
TM
SC
Irkutsk
Baikal Lake
Ulan-Ude
Chita
N52°
L.5
Tu
KhD
Hövsgöl Lake
West Transbaikal
Dz
SB
Ag
Hr
Dr
On
North Mongolia
B
Züünharaa town
L.3
L.1
L.2
MML
L.4
Ulaanbaatar capital city
GK
N48°
Zg
HD
Hh
AH
Tt
L.8
B'
South Mongolia
Ub
CM
E114°
0
200
kilometers
E102°
E108°

◂**Fig. 1** **a** Tectonic zoning of North, Central, and East Asia. *SC* Siberian craton, *EEC* East European craton, *NPC* North China platform, *TB* Tarim block, *CAOB* Central Asian Orogenic Belt. The rocks of CAOB are divided into following belts and plains: the Sayan-Baikal (SB), Altai-Sayan (AS), North Tien Shan (NTS), Mongol–Okhotsk (MO), Gobi-Khingan (GK), South Tien Shan (STS), Junggar-Balkhash (JB), Central Kazakhstan (CK), Ob-Zaysan (OZ), East Ural (EU), Hangai-Daur (HD), Solonker (S) Beishan (B), and Sikhote-Alin (SA) belts and the Amur-Zeya (AZ), Songliao (Sl), Junggar (J), Turan (T), and West Siberian (WS) plains (simplified after Petrov et al. 2014). The Main Mongolian Lineament (MML) marks the border between the AS, SB, and HD belts and the GK belt and is considered as one of the major tectonic lines of the CAOB. **b** Geological outline of North Mongolia–West Transbaikal region. This region is represented by the *black square* in the middle **a**. The terranes in this region are as follows: Central Mongol (CM), Tuva Mongol (TM). Dzhida (Dz), Khamar Daban (KhD), Tunka (Tu), Ikat (Ik), and Eravna (Er) of the SB belt and Zag (Zg), Tsetserleg (Tt), Harhorin (Hh), Haraa (Hr), Asralt Hairhan (AH), Daur (Dr), Aga (Ag), Onon (On), and Ulaanbaatar (Ub) of the HD belt (after Bulgatov and Gordienko 1999; Petrov et al. 2014; Tomurtogoo 2012). The *number* reflects the locality (L) of the Late Paleozoic folds and thrusts: *L.1* the Züünharaa area; *L.2* the Zuunmod area; *L.3* the Bayangol area; *L.4* the Zaamar area; *L.5* the Tunka area; *L.6* the Ul`zutui, Oldynda and Kydzhimit areas; *L.7* the Bagdarin area; and *L.8* the Ulaanbaatar area (compiled by this study with Purevsuren and Narantsetseg 1991; Dejidmaa 2003; Zhimulev et al. 2011; Gordienko et al. 2012; Ruzhentsev et al. 2012; Takeuchi et al. 2012; Altanzul and Baasandolgor 2014). The study area (*black dashed box*) is located within the Haraa terrane (Hr), from Fig. 2, in greater detail

supercontinent Rodinia (e.g., Kovalenko et al. 2004); and (3) the time-stepped collision of various island arcs and the subduction of oceanic crust (Badarch et al. 2002; Xiao et al. 2003; Windley et al. 2007) during the amalgamation of the SC, EEC, NPC, and TB.

The North Mongolia–West Transbaikal region (Fig. 1a, b), which lies north of the Main Mongolian Lineament (MML; Badarch et al. 2002; Tomurtogoo 2006; Kröner et al. 2007; Windley et al. 2007), is one of the significant portions for Paleozoic–Mesozoic tectonics of the CAOB in the Northeast Asia. Geologically, this region is comprised of rocks from the Middle Devonian Sayan-Baikal and Middle–Late Triassic Hangai-Daur belts (Fig. 1b, Petrov et al. 2014). The Paleozoic accretionary complexes (Kurihara et al. 2009; Tomurtogoo 2012) in the Hangai-Daur belt were formed by the northward subduction of the oceanic plate (Mongol Okhotsk oceanic plate; e.g., Tang et al. 2016) beneath the SC (Zorin 1999; Donskaya et al. 2013). The Mongol–Okhotsk Ocean was previously present between the SC and NCP/TB (Fig. 1a, e.g., Enkin et al. 1992; Gordienko 2001; Badarch et al. 2002; Donskaya et al. 2013; Ruppen et al. 2013). However, the closing process and termination of the Mongol–Okhotsk Ocean are still unclear (e.g., Zorin 1999; Kravchinsky et al. 2002; Kelty et al. 2008; Donskaya et al. 2013). Only the closure of the ocean, regarded to be the result of the collision between the SC and the NCP, is generally agreed upon (e.g., Enkin et al. 1992; Kravchinsky et al. 2002; van der Voo et al. 2015; Fritzell et al. 2016).

Studying the geological processes and features from the Paleozoic accretionary complexes to the continental margin of the SC in the North Mongolia–West Transbaikal region will facilitate understanding of the tectonics of the CAOB (Fig. 1b). However, the structural and tectonic aspects in this region remain poorly understood because of a lack of detailed tectonic studies. 3D imaging and structural interpretation are an essential part of establishing the regional tectonic setting of an area. This paper describes the lithology, stratigraphy, geological structure, and U-Pb age of the rocks in the Züünharaa area, about 150 km north of Ulaanbaatar city, Mongolia (Fig. 1b). The Züünharaa area is located within the Haraa terrane of the Hangai-Daur belt, which has a continental affinity. The tectonic implication of the low-angle south-dipping thrust in this area is discussed within the North Mongolia–West Transbaikal region.

Geology

The CAOB (Fig. 1a) is composed of Middle Devonian (Sayan-Baikal, SB; Altai-Sayan, AS; Kazakhstan, K; North Tien Shan, NTS), Late Carboniferous–Permian (Mongol–Okhotsk, MO; Gobi-Khingan, GK; South Tien Shan, STS; Junggar-Balkhash, JB; Central Kazakhstan, CK; Ob-Zaysan, OZ; East Ural, EU), Middle–Late Triassic (Hangai-Daur, HD; Solonker, S; Beishan, B) and Early Cretaceous (Sikhote-Alin, SA) belts and Mesozoic–Cenozoic (Amur-Zeya, AZ; Songliao, Sl; Junggar, J; Turan, T; West Siberia, WS) plains (Petrov et al. 2014). The basement rocks of Mongolia are divided into two regions, North and South, separated by the Main Mongolian Lineament (Fig. 1a; MML; e.g., Badarch et al. 2002; Tomurtogoo 2006; Kröner et al. 2007; Windley et al. 2007). The North Mongolia–West Transbaikal region (Fig. 1b), which lies north of the MML, is divided into the Sayan-Baikal (SB) belt and Hangai-Daur (HD) belt (Fig. 1a, b; Petrov et al. 2014). The SB belt is considered to be a collage of amalgamated blocks that have been accreted to the Siberian craton, while the HD belt is regarded as accretionary complexes with shelf facies rocks (e.g., Kurihara et al. 2009; Tomurtogoo 2012, 2014; Bulgatov and Gordienko 2014).

The SB belt is mainly composed of Precambrian continental basement rocks, Neoproterozoic–Carboniferous sedimentary rocks and Permian–Triassic volcanic–plutonic rock complexes (Bulgatov and Gordienko 1999, 2014; Parfenov et al. 2009; Donskaya et al. 2013). The rocks of SB belt are divided into following seven geological units (Fig. 1b): Central Mongol, Tuva Mongol, Dzhida, Khamar Daban, Tunka, Ikat and Eravna terranes (Parfenov et al. 2004a, 2009; Tomurtogoo 2006, 2012, 2014).

Paleoproterozoic to Early Cambrian metamorphic rocks, ophiolitic rocks, and volcanic-sedimentary rocks are largely exposed in the Central Mongol, Tuva Mongol, Dzhida, and Khamar Daban terranes. The Paleozoic rocks occur in the Tunka, Ikat, and Eravna terranes (Parfenov et al. 2004a, 2009). The Permian–Triassic volcanic–plutonic rock complexes overlap the rocks of the SB belt and form the Selenga superimposed volcano–plutonic belt (Fig. 1b; Bulgatov and Gordienko 1999, 2014; Parfenov et al. 2004b, 2009).

The Central Mongol and Tuva Mongol are considered to be Precambrian continental fragments, while the Dzhida and Khamar Daban terranes are regarded to be Early Paleozoic accretion–collision orogens with a complex N-verging fold-thrust structure (e.g., Tomurtogoo 2006; Belichenko et al. 2003; Gordienko et al. 2007). The Tunka terrane is located on the west side of the southern rim of the Siberian craton (Fig. 1b). This terrane consists mainly of Ordovician–Silurian terrigenous-volcanogenic-carbonate sedimentary rocks and is intruded by Tunka granite of the Sarkhoi plutonic complex with an U-Pb age of 462.6 ± 7.8 Ma (Zhimulev et al. 2011). The molasses-like Late Devonian–Early Carboniferous Sagan-Sair Formation overlaps the Tunka granite and Ordovician–Silurian sedimentary rocks (Buslov et al. 2009; Zhimulev et al. 2011). The rocks of the Tunka terrane form a complex N-verging fold-thrust structure (e.g., Ryabinin et al. 2011; Zhimulev et al. 2011).

The rocks of the Ikat and Eravna terranes occur as scattered fragments or variable size of xenoliths in the Angara-Vitim batholith (Donskaya et al. 2013) of the Permian–Triassic superimposed volcanic–plutonic rock complexes (Fig. 1b, e.g., Parfenov et al. 2009; Badarch 2005; Ruzhentsev et al. 2012). The Ikat and Eravna terranes are primarily composed of Neoproterozoic–Carboniferous weakly metamorphosed carbonate-terrigenous deposits with minor volcanogenic rocks (Mazukabsov et al. 2010). The Neoproterozoic–Carboniferous rocks form a complex N-verging fold-thrust structure in the Ul'zutui, Oldynda, Kydzhimit areas of the Eravna terrane and the Bagdarin area of the Ikat terrane (Ruzhentsev et al. 2006, 2012).

The HD belt is largely composed of Cambrian–Ordovician proximal shallow marine sedimentary rocks and Paleozoic accretionary complexes (Tomurtogoo 2006, 2012; Kurihara et al. 2009). The Paleozoic rocks of the HD belt are divided into the following nine geological units (Fig. 1b): Zag, Tsetserleg, Harhorin, Haraa, Asralt Hairhan, Daur, Aga, Onon, and Ulaanbaatar terranes (Bulgatov and Gordienko 1999, 2014; Tomurtogoo 2012, 2014). Most terranes in the HD belt are regarded as accretionary complexes, with the exception of the Zag and Haraa terranes. The Ulaanbaatar terrane (late Devonian Early Carboniferous accretionary complex) is composed mainly of basalts, limestone, Silurian–Devonian radiolarian chert, siliceous mudstone, and clastic rocks (e.g., Kurihara et al. 2009; Nakane et al. 2012; Suzuki et al. 2012; Takeuchi et al. 2012; Tsukada et al. 2013). The Ulaanbaatar, Harhorin, and Tsetserleg terranes are structurally and lithostratigraphically correlative (Kurihara et al. 2009; Purevjav and Roser 2013; Tsukada et al. 2013). The Asralt Hairhan terrane is considered to have a metamorphic affinity to the Ulaanbaatar terrane (e.g., Tomurtogoo 2012; Gordienko et al. 2012). The Daur, Aga, and Onon terranes consist of accretionary complexes dominated by deformed–metamorphosed mélanges containing fragments of ophiolite, arc-related volcanic, and sedimentary rocks with minor amounts of radiolarian chert and limestone (Bulgatov and Gordienko 1999; Zorin 1999; Badarch 2005; Tomurtogoo 2012).

The Zag terrane consists of highly deformed pelitic and psammitic schist of the Zag Group, which yielded K-Ar ages of 459.9 ± 9.1 and 447.4 ± 9.0 Ma (Kurimoto et al. 1998; Badarch 2005). The Haraa terrane (Fig. 1b) is largely composed of Cambrian–Lower Ordovician metamorphosed clastic rocks of the Haraa Group (Tomurtogoo 2006, 2012). The rocks of the Haraa Group are intruded by the Boroogol plutonic rock complex giving the U-Pb age of 460–440 Ma (e.g., Kröner et al. 2007; Hou et al. 2010). The Haraa Group and Boroogol plutonic rock complexes are unconformably overlain by Devonian–Permian volcanic and clastic rocks (Badarch et al. 2002). The younger Paleo-Mesozoic plutonic rocks intrude into the above sedimentary and igneous rocks (Tomurtogoo 2006; Donskay et al. 2013).

The bedding and structural planes in the Zag and Tsetserleg terranes generally trend northwest and steeply dip north- or southward, west of the HD belt (e.g., Badarch et al. 2002; Buchan et al. 2001; Purevjav and Roser 2013; Tsukada et al. 2013), whereas those in the Haraa, Asralt Hairhan, Ulaanbaatar, Daur, and Aga terranes trend northeast and steeply dip northward in the east (e.g., Zorin 1999; Kurihara et al. 2009; Takeuchi et al. 2012). The rocks of the Harhorin terrane trend north-northwest and dip southwestwardly in fault contact with the Tsetserleg terrane in the west by the northwestwardly trending fault system (Fig. 1b; Tseden et al. 1992; Tsukada et al. 2010; Purevjav and Roser 2013). The rocks of the Onon and Aga terranes form an S-like bowing structure, elongating to northeast and dipping northward (Fig. 1b, e.g., Zorin 1999). The rocks of the Asralt Hairhan and Ulaanbaatar terranes form southeast-verging composite folds associated with northward-dipping thrusts (e.g., Kurihara et al. 2009; Gordienko et al. 2012; Nakane et al. 2012; Suzuki et al. 2012; Takeuchi et al. 2012). The Asralt Hairhan terrane is in fault contact with the Haraa terrane via the northeastwardly trending Late Mesozoic Yeroogol sinistral strike-slip fault system at its

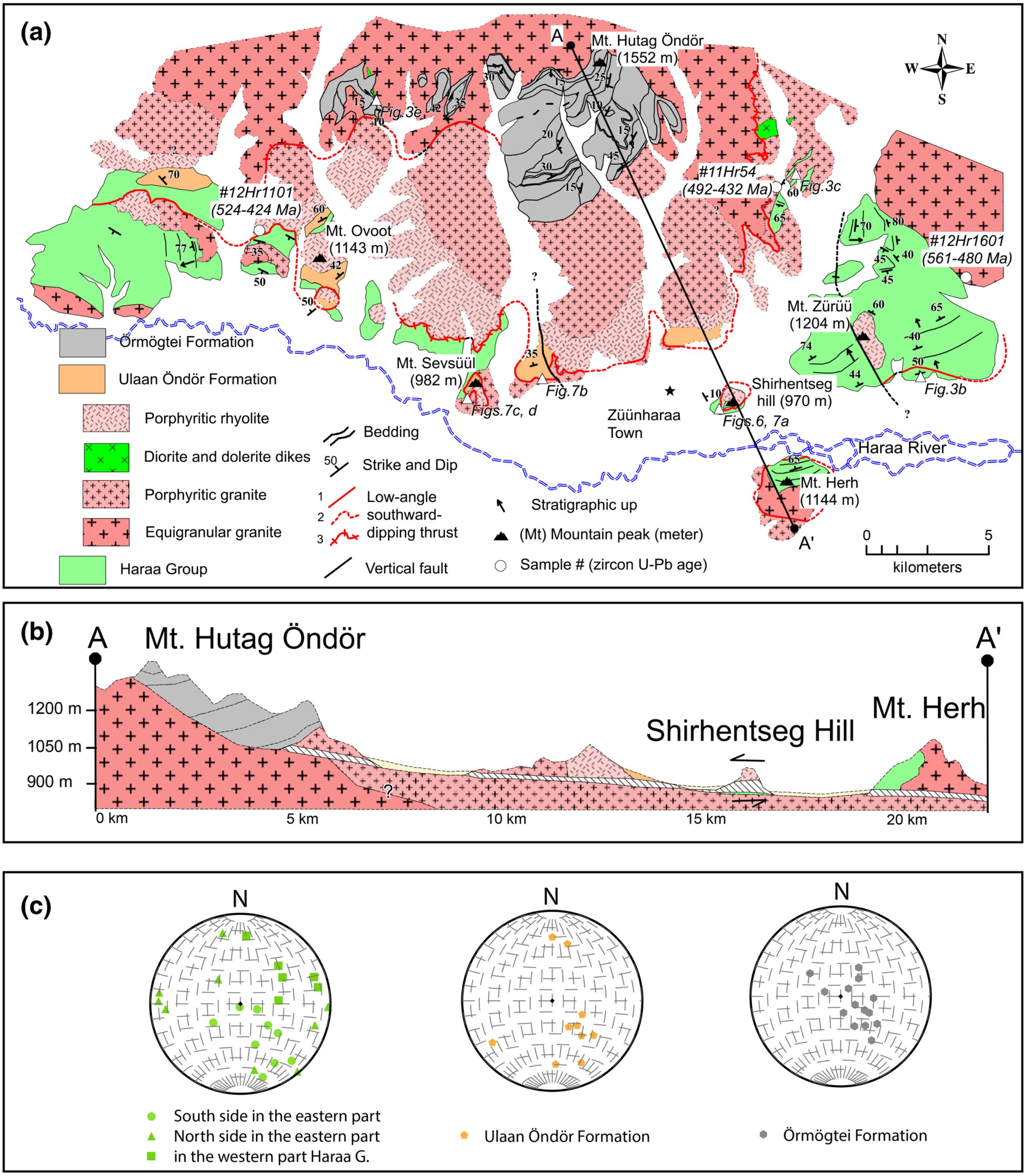

Fig. 2 **a** Geological map around the Züünharaa area. *Red lines* are low-angle southward-dipping thrust: (1) conformed; (2) concealed; and (3) inferred. Circle points are the location of samples with zircon U-Pb age. *Triangle points* are the location of outcrops, which are shown in Figs. 3a–d, 6a–d, and 7a–d. **b** Geological cross section along *AA'*. **c** Bedding planes of rocks in the Haraa Group, Ulaan Öndör Formation, and Örmögtei Formation by pole on the Stereonet diagram

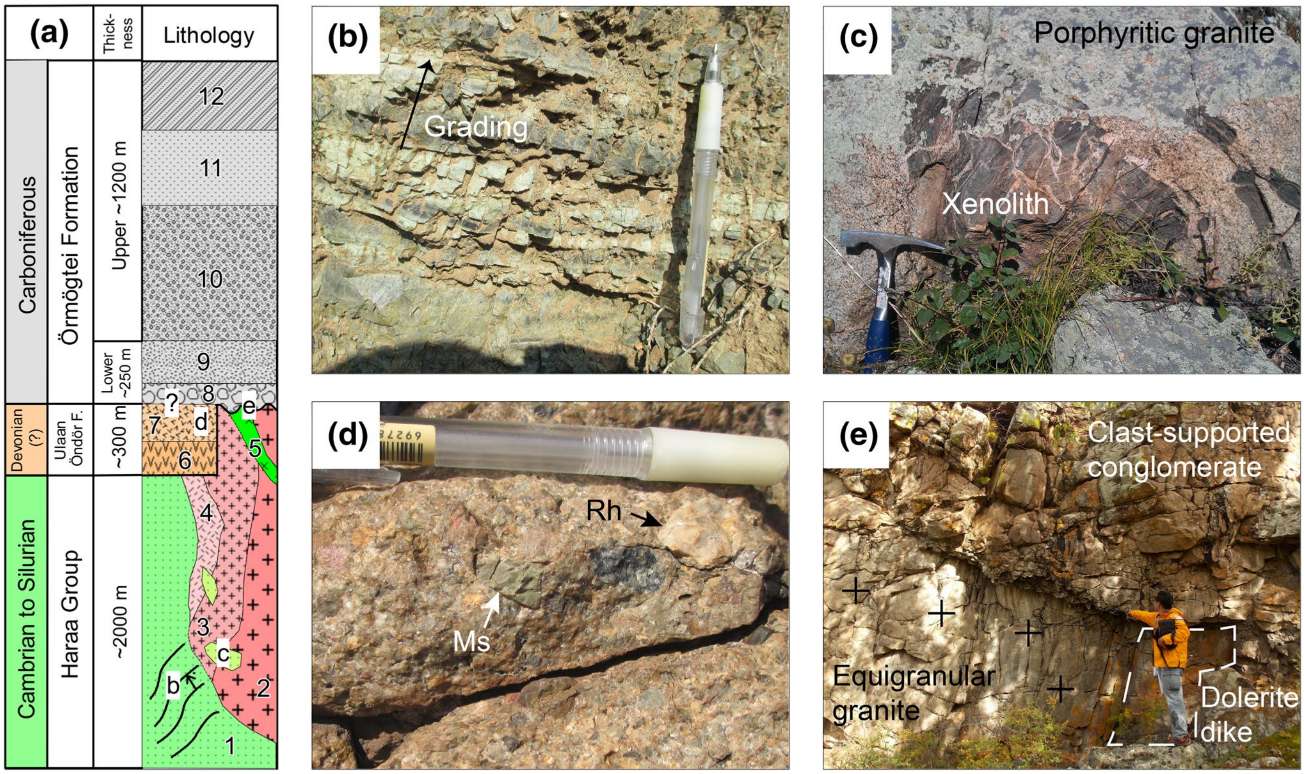

Fig. 3 Generalized lithostratigraphic column with field occurrence of distributed rocks in the Züünharaa area. **a** Rocks are as follows: (1) metamorphosed sandstone–mudstone; (2) equigranular granite; (3) porphyritic granite; (4) porphyritic rhyolite; (5) diorite–dolerite dikes; (6) dacitic to rhyolitic lava; (7) tuff breccia; (8) clast-supported conglomerate; (9) arkosic sandstone; (10) matrix-supported conglomerate; (11) bedded sandstone; and (12) alternating beds of mudstone and sandstone. **b** Dark-light banded beds of the metamorphosed sandstone–mudstone showing a stratigraphic up (*black arrow*). **c** Xenolith from the Haraa Group in porphyritic granite shows evidence of intrusion. **d** Angular to sub-rounded clasts of rhyolitic to dacitic lava, porphyritic granite–rhyolite (Rh), and the metamorphosed sandstone–mudstone (Ms) are included in the tuff breccia, indicating conformity. **e** Equigranular granite is intruded by dolerite dike and is unconformably overlain by basal clast-supported conglomerate; and the co-author pinpoints the unconformity. The length of a mechanical pencil, a hammer, and the height of the co-author denote 14.5, 20, and 170 cm, respectively

northern end (Fig. 1b; Tseden et al. 1992; Kotlyar et al. 1998; Altanzul and Baasandolgor 2014).

The study area (L.1, Fig. 1b) is located within the Haraa terrane and includes Züünharaa Town, Mongolia. The study area exposes metamorphosed clastic rocks of the Haraa Group, volcanic rocks of the Ulaan Öndör Formation, and clastic rocks of the Örmögtei Formation in ascending order (Figs. 2, 3). The rocks of the Haraa Group are intruded by granitic rocks. A part of the granitic rock is monzogranite according to the I.U.G.S. classification of plutonic rocks (Streckeisen and Le Bas 1991). The granitic rock gradually changes into finer rhyolitic rocks in places and is intruded by later dikes of diorite and dolerite (Figs. 2, 3). Tomur et al. (1994) defined the volcaniclastic rocks in the Zuunmod area, 30 km south from the study area (L.2, Fig. 1b), as Devonian Ulaan Öndör Formation. The volcaniclastic rocks in the study area are regarded as equivalent to the Ulaan Öndör Formation based on their lithological similarity (Purevsuren and Narantsetseg 1998). The clastic rocks of the Örmögtei Formation unconformably overlie the granitic rock with basal conglomerate (Figs. 2a, b, 3d).

Methods and samples

We carried out field research on a 600 km^2 area in and around Züünharaa Town to detail the lithology, stratigraphy, and geological structure (Figs. 2, 3, 4, 5, 6, 7, 8). The obtained data are used to examine tectonics of the SB and HD belts. Based on the obtained data, the geological map and cross section are newly established.

Zircon LA–ICP–MS dating of the granitic rock was carried out for a sample from equigranular granite (#12Hr1601) and two samples from porphyritic granite–rhyolite (#11Hr54 and #12Hr1011) to constrain geological framework of the study area (Fig. 2a). Sample preparation for U-Pb dating of zircons by LA–ICP–MS is described in Chang et al. (2006). The zircon samples were concentrated using the conventional mineral-separation

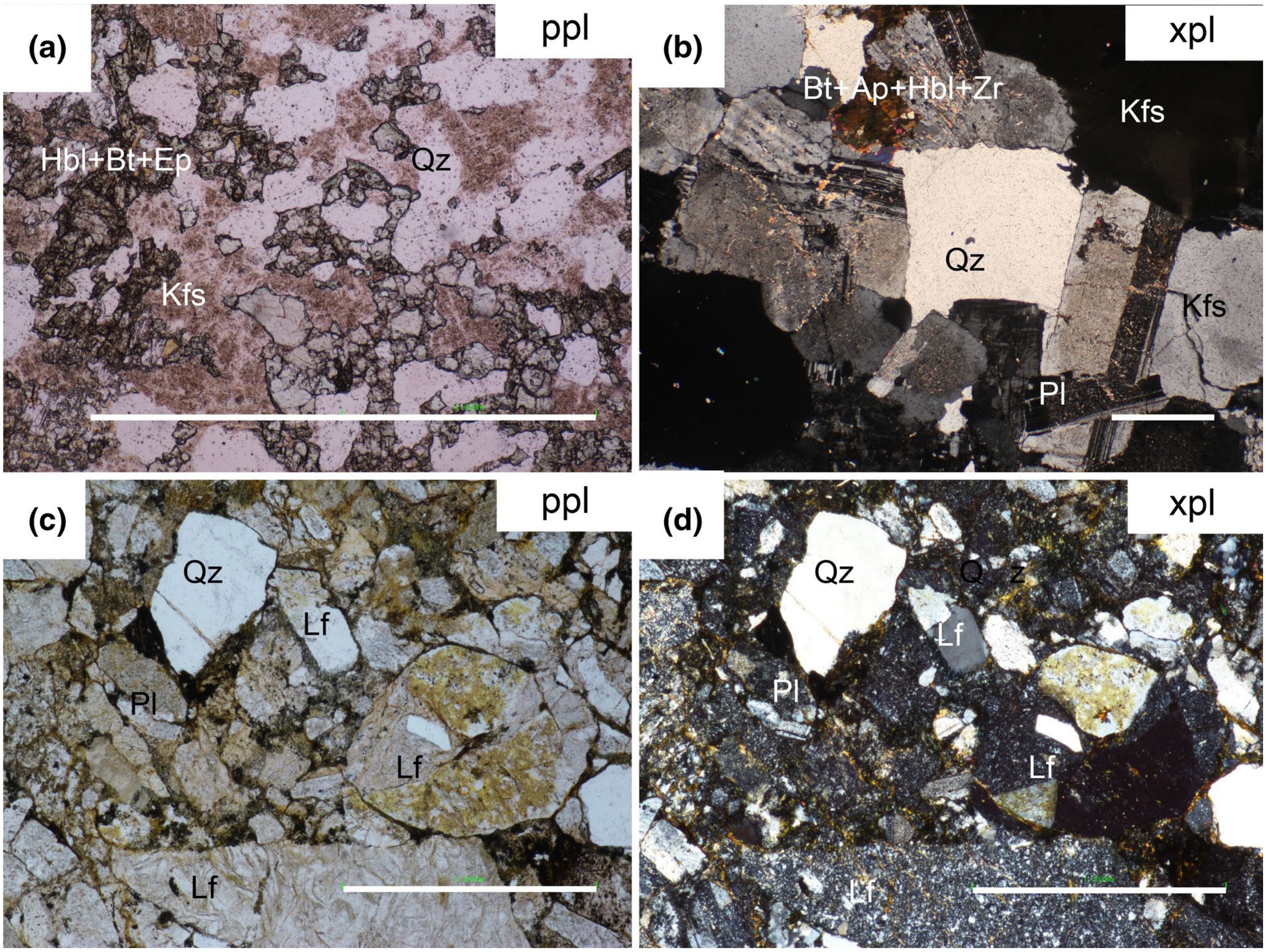

Fig. 4 Photomicrographs of thin sections from distributed rocks in the study area. **a** Metamorphosed sandstone from the Haraa Group. Abundant hornblende, biotite, and episode occur in a finer matrix of fine-grained sandstone. **b** Equigranular granite. Magmatic zircons are included in the biotite, aplite, and hornblende. **c, d** Bedded sandstone from the Örmögtei Formation. Abundant lithic fragments are derived from igneous rocks and are included in the bedded sandstone. Abbreviations on photomicrographs: quartz (Qz), K-feldspar (Kfs), plagioclase (Pl), hornblende (Hbl), biotite (Bt), epidote (Ep), apatite (Ap), zircon (Zr), lithic fragment (Lf), plane-polarized light (ppl), AND cross-polarized light (xpl). The *white line* denotes 1 mm

techniques, including crushing and pulverizing, followed by separation (by hand) using magnets. These zircon grains were then mounted in an epoxy resin, and diamond polished to expose the interior. To investigate the internal structure of the individual grains, a scanning electron microscope (SEM; Hitachi S-3400N equipped with Gatan MiniCL) installed at Nagoya University was used to obtain backscattered electron (BSE) and cathode luminescence (CL) images.

The analyzed zircon grains are colorless, 50–100 μm in length along their major axes and have a length-to-width ratio of 1.5–2. These zircon grains mostly occur as subhedral to euhedral prisms, and contain distinct cores with concentric zoning, consistent with crystallization from a viscous magma, and overgrowths (Fig. 9a–d, e.g., Corfu et al. 2003).

The samples were analyzed by Inductively Coupled Plasma Mass Spectrometry (Quadrupole type ICP-MS; Agilent 7700x), which was connected with the NWR-213 LA system (Electro Scientific Industries, Inc.) installed at Nagoya University. The ablation pit size was 25 μm under conditions of 10 Hz repetition rates with energy densities of ~12 J/cm^2. Materials used for calibration were 91,500 standard zircon (1062.4 Ma; Wiedenbeck et al. 1995) and silicate glass reference materials produced by the National Institute of Standards and Technology (NIST): SRM 610 (Horn and Von Blanckenburg 2007). Further details on the accuracy and reproducibility of U-Pb can be found in Orihashi et al. (2008), Iwano et al. (2013) and Kouchi et al. (2015).

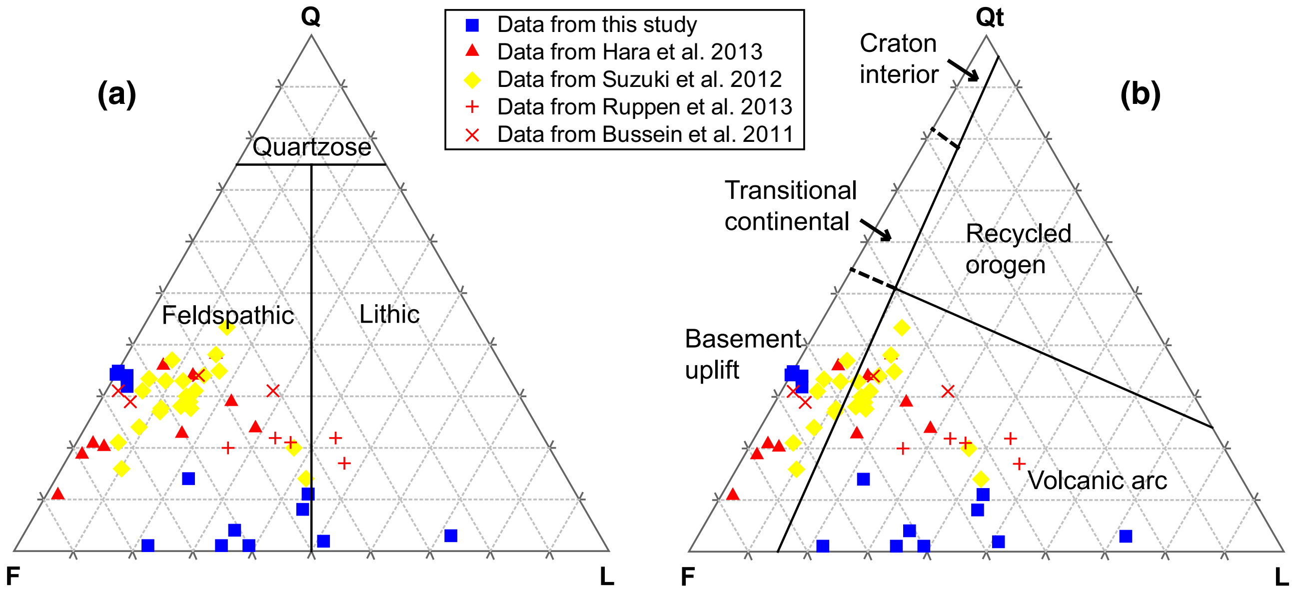

Fig. 5 Petrographic classification and provenance of sandstone from the Örmögtei Formation. **a** Q–F–L diagram from Okada 1971 and **b** Qt–F–L from Dickinson et al. (1983). Sandstone from the Örmögtei Formation is classified as feldspathic arenite and are plotted in the field of "basement uplift" and "volcanic arc". Carboniferous sandstone results of Bussien et al. (2011), Hara et al. (2013), Ruppen et al. (2013), and Suzuki et al. (2012) are plotted for comparison. Total quartz (mono- and polycrystalline grains; Qt), feldspars (plagioclase and potassium feldspar; F), and lithic fragments (L)

Detailed geology of the study area

Lithology and stratigraphy

(1) Haraa Group

The rocks of the Haraa Group consist of metamorphosed sandstone with mudstone intercalations (Fig. 3a, b). Sandstone is usually fine- to medium-grained, sub-angular, generally well-sorted but poorly sorted in some horizons. It includes many grains of quartz and feldspar in a finer matrix. Hornblende, amphibole, biotite, chlorite, and epidote occur in the rocks as metamorphic minerals (Fig. 4a). The alternating beds of sandstone and mudstone show sedimentary structures, such as graded bedding (Fig. 3b), cross bedding, and load casts in some places. The thickness of a bed varies from several millimeters to several meters. Several xenoliths, which are derived from metamorphosed sandstone–mudstone, are observed in the granitic rocks (Fig. 3c). The total thickness of the metamorphosed clastic rocks exceeds 2000 m (Fig. 3a).

(2–4) Granitic rocks and (5) mafic dikes

In this study, the granitic rock is subdivided into three types based on texture: (2) equigranular granite (monzogranite), (3) porphyritic granite, and (4) porphyritic rhyolite (Figs. 2a, 3a). The equigranular granite generally includes K-feldspar and plagioclase as major minerals, and minor amounts of quartz, hornblende, biotite, apatite, and zircon (Fig. 4b). The major minerals are 1–3 mm in size. Subhedral to euhedral K-feldspar shows micro-perthite texture and twinning with sericite inclusion. Plagioclase shows that clear stripe twining is often turbid in the interior, owing to alteration (Fig. 4b). Hornblende and biotite, displaying brown under plane-polarized light, occur as slender needles or lathes.

The porphyritic granite is inter-gradual with porphyritic rhyolite, and the boundary between them is obscure (Fig. 2a, b). Porphyries of quartz, K-feldspar, and plagioclase, up to 7 mm in size, are embedded in a finer groundmass in the porphyritic granite. Minor amounts of amphibole, biotite, and sericite are also included in the porphyritic granite. Some porphyritic granite has abundant crystals of sphene, zircon, and opaque minerals. The porphyritic rhyolite includes phenocrysts of quartz and feldspar in a microcrystalline groundmass. Phenocrysts are up to 3 mm in size. Biotite and hornblende, up to 0.5 mm in size, also occur in a groundmass.

Small dikes of (5) diorite and dolerite intrude into the porphyritic granite and equigranular granite (Figs. 2a, 3e). The diorite is composed of plagioclase, hornblende with a small amount of K-feldspar, biotite, and sphene. The dolerite includes phenocrysts of plagioclase, augite and quartz in a finer groundmass of intersertal plagioclase.

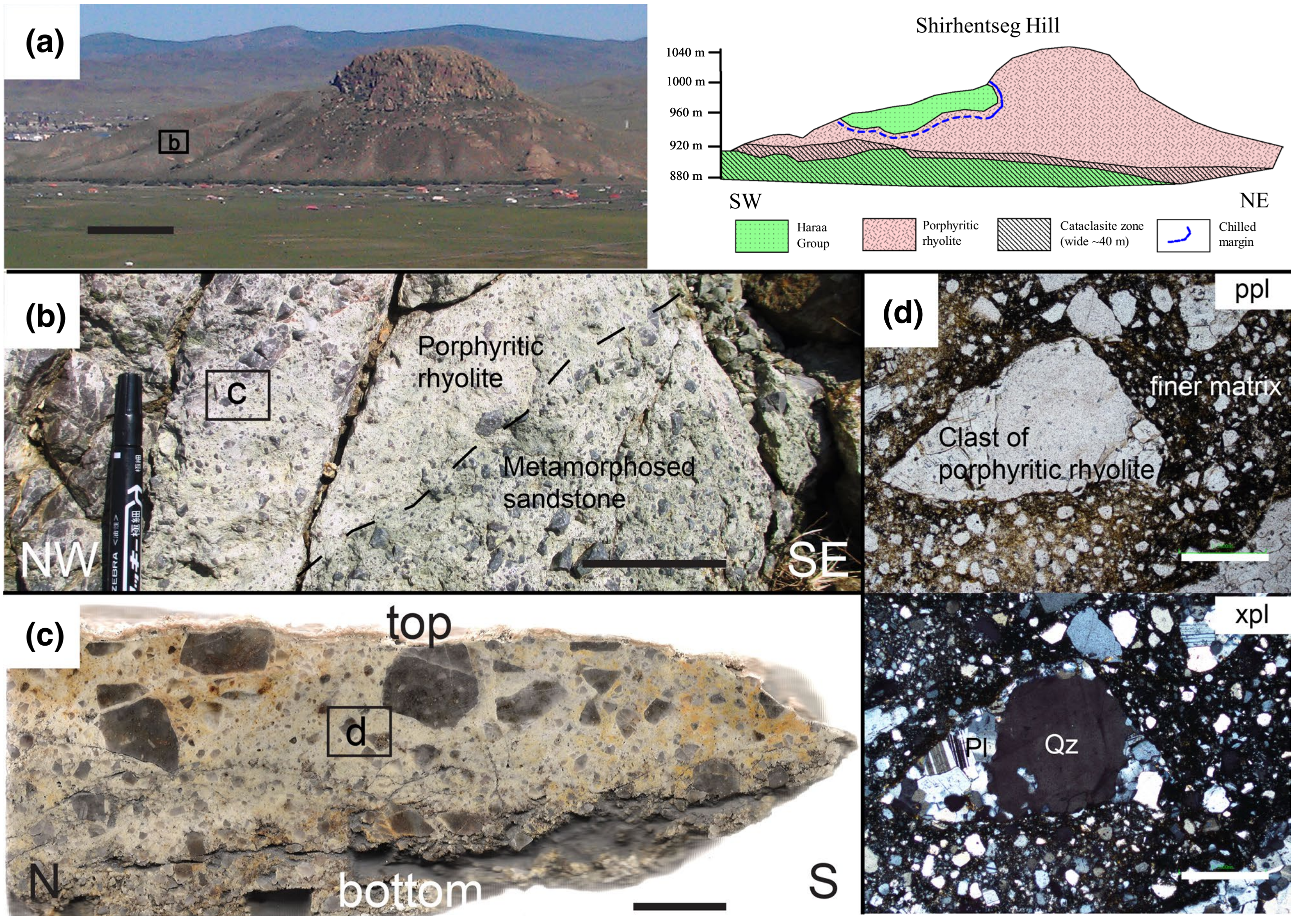

Fig. 6 Occurrence of cataclasite rocks in and around of the low-angle southward-dipping thrust at different scales. *Boxes* are the approximate location of the following figures. *Scale lines* denote ca. 100 m, 5 cm, 1 cm, and 0.5 mm, for views **a**–**d**, respectively. **a** Porphyritic rhyolite overthrust onto the Haraa Group to form a cataclasite zone, more than 40 m wide at Shirhentseg hill, east of Züünharaa Town. **b** Rock outcrop shows an intensively sheared part of the cataclasite zone; the *dashed line* marks a lithological boundary between the porphyritic rhyolite and the metamorphosed sandstone of the Haraa Group. **c** Polished surface of a rock sample of non-foliated cataclasite along an oriented cut. **d** Photomicrographs show an angular clast, which is derived from porphyritic rhyolite. Abbreviations on photomicrographs: quartz (Qz), K-feldspar (Kfs), plagioclase (Pl), plane-polarized light (ppl), and cross-polarized light (xpl)

(6–7) Ulaan Öndör Formation

The rocks of the Ulaan Öndör Formation overlie the rocks of the Haraa Group and the granitic rocks (Figs. 2a, b, 3a). This formation is composed mainly of (6) rhyolitic–dacitic varicolored lava and (7) tuff breccia, in ascending order (Fig. 3). The lava includes irregular-shaped phenocrysts of quartz and feldspar in a cryptocrystalline groundmass. The tuff breccia is yellowish green, clast-supported and poorly sorted, and intercalates fine- to medium-grained tuffaceous mudstone layers in some horizons. Tuff breccia includes angular to sub-rounded clasts of rhyolite–dacite, porphyritic granite–rhyolite, and metamorphosed sandstone–mudstone (Fig. 3c). The clasts are up to 10 cm in size. Tuffaceous mudstone rarely contains quartz and plagioclase in a finer matrix. The total thickness exceeds 300 m (Fig. 3a).

(8–12) Örmögtei Formation

The clastic rocks of the Örmögtei Formation unconformably overlie the equigranular granite (Figs. 2a, b, 3a, e). This formation is subdivided into the lower and upper members. The lower member consists of (8) clast-supported conglomerate and (9) medium- to coarse-grained massive arkosic sandstone and the upper member consists of (10) matrix-supported conglomerate, (11) fine- to medium-grained bedded sandstone, and (12) alternating beds of mudstone and sandstone, in ascending order (Fig. 3a).

Clast-supported conglomerate includes abundant boulders, up to 5 m in size, of porphyritic granite–rhyolite. Arkosic sandstone is largely composed of quartz and feldspar grains and includes clasts of cobble- to pebble-sized, rounded porphyritic rhyolite.

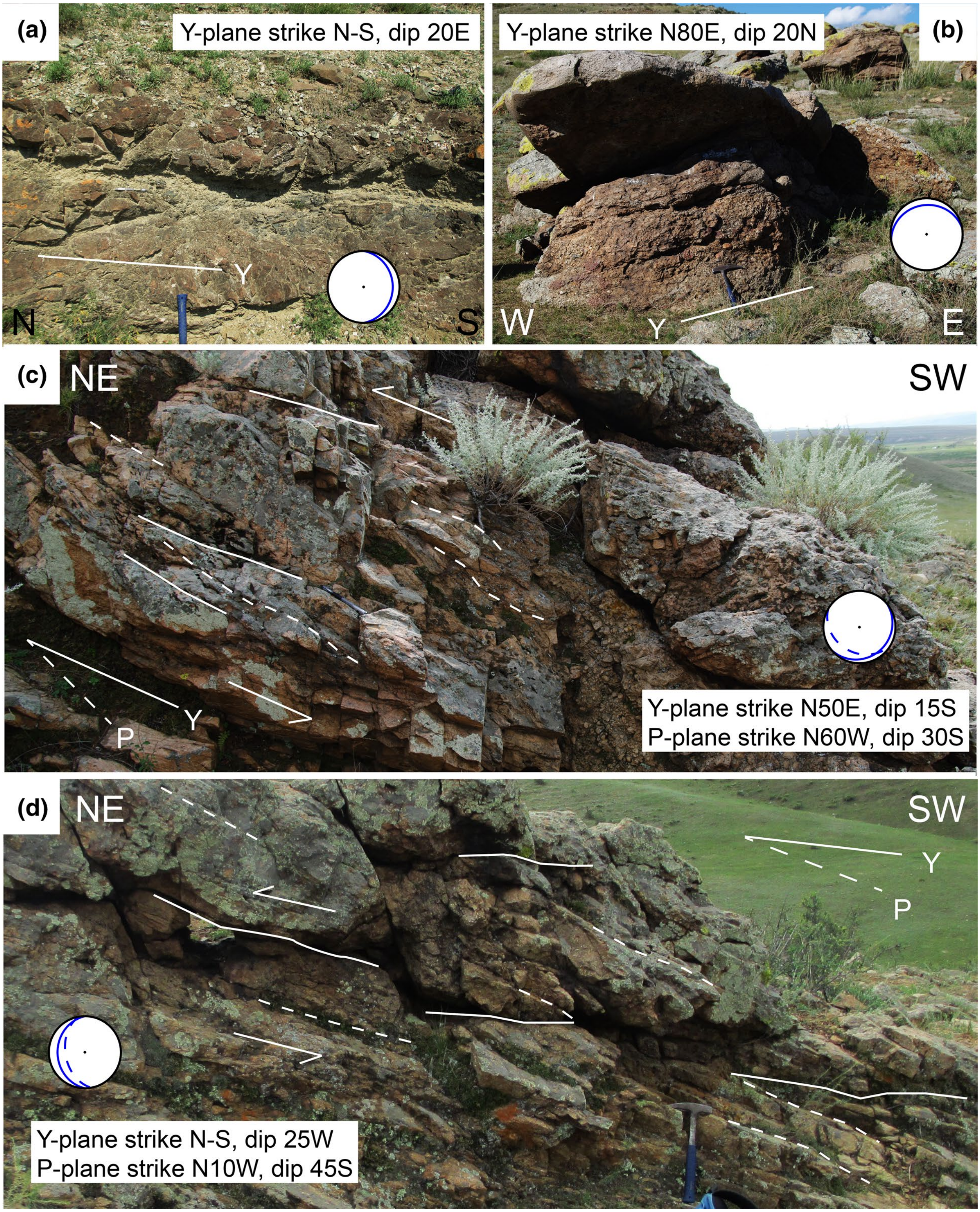

Fig. 7 Representative outcrops of foliated cataclasite from the low-angle southward-dipping thrust. Sub-horizontal cataclasites exposed in many places. Locations are shown in Fig. 2a and in Table 1. Solid lines represent Y-planes, and dashed lines are P-planes. Shear sense (*arrow*) was determined from the Y–P composite planar planes. The great circles in the lower hemisphere projection show the Y–P planes of the outcrop. **a** Rock outcrop of metamorphosed sandstone from the Haraa Group shows a sub-horizontal fault plane. **b** Sub-horizontal cataclasited section of the tuff breccia shows few Y-planes. Outcrops **c, d** are foliated cataclasite derived from porphyritic granite–rhyolite showing several Y–P planes, which suggest top-to-the-north shearing

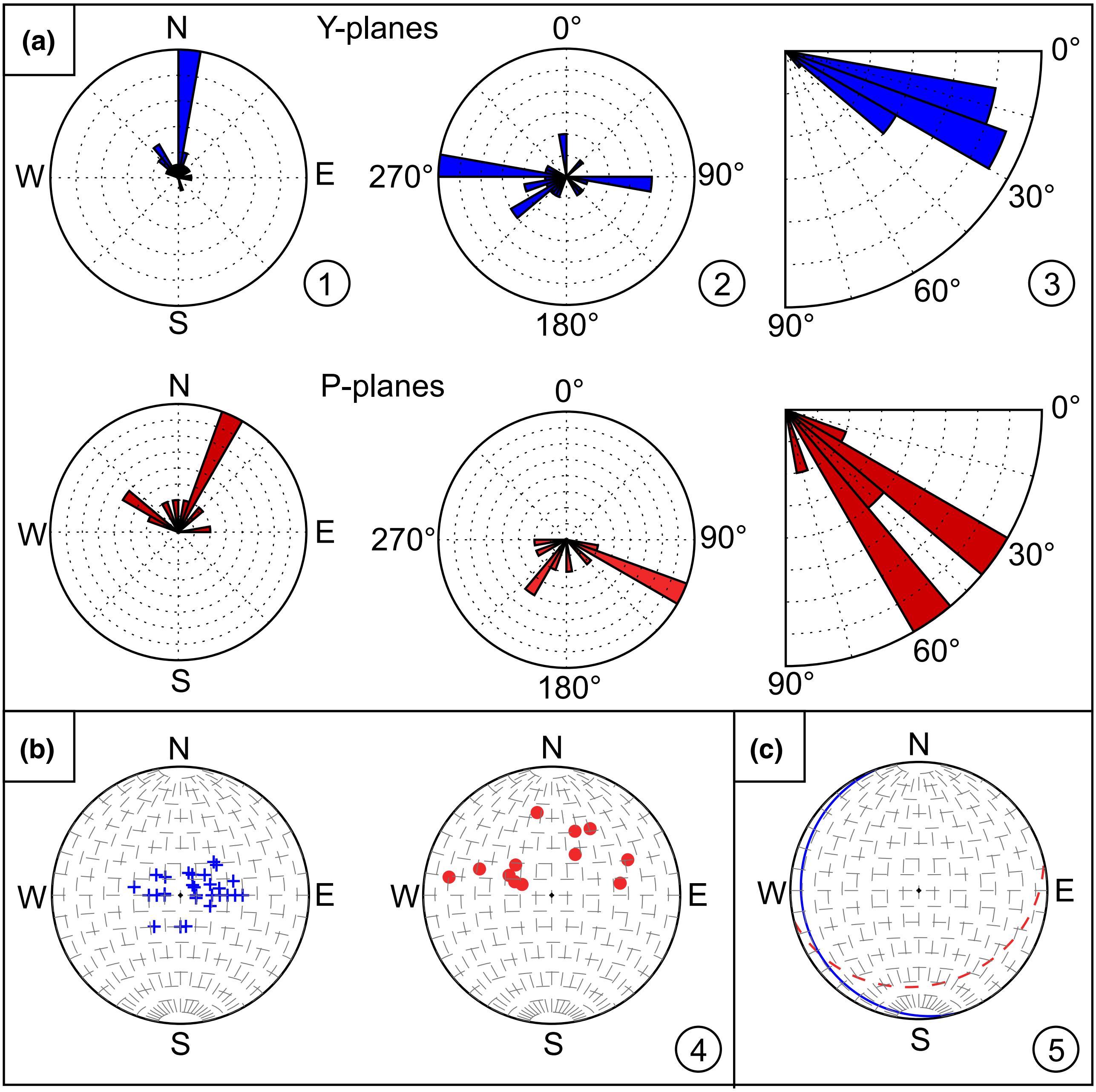

Fig. 8 Orientation data for all Y–P planes measured from several outcrop surface exposures of the low-angle southward-dipping thrust in the study area. **a** Rose diagrams by (1) data from the strike; (2) dip direction; and (3) dip angle of the Y–P planes. **b** Stereonet diagram by (4) data from poles of the Y–P planes. The Y-planes and P-planes are represented by blue pluses and red dots, respectively. **c** Stereonet diagram by (5) data from the main thrust plane. The *great blue circle* (*solid*) is the main Y-plane, and the great *red circle* (*dashed*) is the average P-plane. The main Y-plane and average P-plane (5) suggest top-to-the-north shearing. The orientation data refer to Table 1

The matrix-supported conglomerate overlies the arkosic sandstone. The matrix-supported conglomerate intercalates the upper part of the bedded sandstone. The bedded sandstone dominated by quartz, plagioclase, potassium feldspar, and rock fragments (Fig. 4c, d) is overlain by the alternating beds of mudstone and sandstone. The sandstone of the alternating beds is composed largely of quartz, plagioclase and potassium feldspar, and rock fragments. Each bed is several centimeters thick. Sedimentary structures, such as graded bedding and cross lamina in the alternating beds, show stratigraphic up (Fig. 2a). The sandstone is classified as feldspathic arenite in the Q–F–L diagram (Fig. 5a; Okada 1971). In the Qt–F–L diagram (Dickinson et al. 1983), this sandstone is plotted in the field of "basement uplift" and "volcanic arc" (Fig. 5b). The sandstone has clasts of rhyolitic tuff and also includes lesser amounts of zircon, muscovite, biotite, epidote, and chlorite (Fig. 4c, d). Some mudstone layers in the alternating beds yield brachiopod fossils. The type section of the Örmögtei Formation, 45 km north from the study area, is assigned to the Visean based on a flore and a brachiopod assemblage, *Tomiodendron ex gr.kemerovience* and *Dyscritella mergensis–Lanopora mongolica* respectively (e.g., Ariunchimeg 2011; Tolokonnikova et al. 2014). Therefore, it is likely that the Örmögtei Formation in this area is also Visean. The total thickness of this formation exceeds 1450 m (Fig. 3a).

In conclusion, the study area can be divided into four types of rocks, i.e., the metamorphosed clastic rocks of Haraa Group, granitic rocks with mafic dikes, the volcanoclastic rocks of the Ulaan Öndör Formation, and the clastic rocks of the Örmögtei Formation (Figs. 2a, 3a), which are subdivided into 12 distinguishable lithological units (Fig. 3a). The Haraa Group intruded via granitic rocks and unconformably covered the Ulaan Öndör and Örmögtei formations. The relationship between the Ulaan Öndör Formation and the Örmögtei Formation is not clear due to poor exposure in the study area, and is inferred to have conformity based on Tomur et al. (1994).

Structure

The rocks of the Haraa Group are exposed in the western and eastern parts of the study area (Fig. 2a). The bedding planes of the rocks trend northwesterly and steeply dip southward to take a monoclinal structure in the western part (Fig. 2c). In the eastern part, the southern side strikes N40°–60°E and dips 40°–65°N, and the northern side strikes N40°W–N10°E and dips 45°–80°N to take a complex fold structure (Fig. 2a, c). The rocks of the Ulaan Öndör formation occur in several small areas at central and western parts of the study area (Fig. 2a). The bedding planes of the volcanoclastic rocks strike N60°E and dip 35°–45°N (Fig. 2a, c). The Örmögtei Formation is open folded with a low-angle axis plunging westward (Fig. 2a). The southern wing strikes N 30°–50°E and dips 15°–45°N, and the northern wing strikes N 45°–60°W and dips 15°–35°S to take a syncline structure (Fig. 2a, c).

We identified a regional low-angle thrust trending E–W and dipping gently southward. The thrust cuts all geologic units throughout in this area with the exception of the Örmögtei Formation (Fig. 2a, b). The rocks in and around the thrust were intensely fractured, forming a cataclasite zone (Fig. 6a). A cataclasite zone with a maximum width of 40 m extends for at least 30 km along the W–E and 20 km along the S–N and exposes from the 900 to 1000 m elevations (Figs. 2a, 6a).

Abundant angular clasts derived from the host rocks, such as meta-sandstone, porphyritic rhyolite–granite, volcaniclastic rocks, and others, are included in a finer matrix, demonstrating the random fabric of the cataclasite (Fig. 6b, c). The cataclasite is rarely foliated in places but generally non-foliated. The clasts are formless, lenticular, spherical, or tabular, and vary in size from several millimeters to several centimeters (Fig. 6c, d). The clasts (>2 mm) make up to 60% of total the volume (Fig. 6c). The cracks in the clasts are filled by grains fed from the matrix. The matrix of the cataclasite is entirely composed of cryptocrystalline minerals (Fig. 6d) derived from host rocks and minor amounts of secondary chlorite, calcite, and sericite (excluding epidote) which suggests a formation temperature above 200 °C (Henley and Ellis 1983). The matrix, which includes cement, occupies more than 40% of the total volume. According to the classification of fault rock by Woodcock and Mort (2008), the rocks in and around the thrust in this area are chaotic breccia and protocataclasite. Textures formed by cataclastic flow and pressure solution are usually observed, and no evidence of ductile deformation, such as grain boundary migration, sub-grain rotation, bulging, and undulose extinction, is observed. Taking into consideration that cataclasites generally occur at conditions lower than 4 kbar (Passchier and Trouw 1998), the present cataclasite without epidote seems to have been formed under conditions of less than 200 °C and 4 kbar.

The foliated cataclasite shows composite planar structures, such as Y- and P-planes of subsidiary fractures or so-called Riedel shears (Riedel 1929). The Y- and P-planes (e.g., Tchalenko and Ambraseys 1970; Bartlett et al. 1981) are defined by thin layers, several millimeters wide, of the clay minerals in parallel orientations (Fig. 7a–d; similar to observations from other brittle shear zones in Mukherjee 2012, 2013a, 2014, 2015). The respective spacing of the Y- and P-planes is ~40 and ~10 cm. The Y-and P-planes generally strike N40°W–N10°E and N50°W–N30°E and dips 10°–35° and 30°–60° (Table 1; Fig. 8a). The assembled data of the Y-plane show generally sub-horizontal planes (Fig. 8b). It suggests that the main fault plane strike ~N18°W and dip 9°S in the study area (Fig. 8c). The average P-plane strikes N76°E and dip 27°S (Fig. 8c). The angle between Y- and P-planes is ~20° (Figs. 7c, d, 8a). Shear sense is determined from the Y–P planes (as in Mukherjee 2010a, b; Mukherjee and Koyi 2010a, b; Misra and Mukherjee 2016; Babar et al. 2016; Kaplay et al. 2016). Shear heating (e.g., Mukherjee 2017) was not manifested in these shear zones (Mukherjee and Mulchrone 2013; Mulchrone and Mukherjee 2015, 2016). The Y–P planes in the foliated cataclasite indicate top-to-the-north shear (Figs. 7c, d, 8c). The cataclasites in the northwestern area discontinue in the east, and the clastic rocks of the Örmögtei Formation were not affected by shearing (Fig. 2a). Two

Table 1 Orientation data of the Y–P planes from the low-angle southward-dipping thrust in the Züünharaa area

Location of fault plane	Y-plane			By pole (4)		P-plane			By pole (4)	
	Strike (1)	Dip direction (2)	Dip (3)	Bearing	Plunge	Strike (1)	Dip direction (2)	Dip (3)	Bearing	Plunge
N48.8489; E106.49[e]	S20E	S70W	20S	70	70	–	–	–	–	–
N48.8489; E106.49	NS	E	15E	270	75	–	–	–	–	–
N48.8489; E106.49	N20E	N70W	20N	110	70	–	–	–	–	–
N48.8489; E106.49	EW	N	20N	180	70	–	–	–	–	–
N48.8489; E106.49	N50W	N40E	26N	220	64	–	–	–	–	–
N48.8489; E106.49	N10W	S80W	25W	80	65	–	–	–	–	–
N48.8504; E106.49	N05E	S85E	10W	275	80	–	–	–	–	–
N48.8471; E106.491[a]	NS	E	20E	90	50	–	–	–	–	–
N48.8572; E106.3916[b]	N80E	N10W	20N	170	20	–	–	–	–	–
N48.8624; E106.3958	N10E	S80E	30S	280	60	N20E	S70E	50S	290	40
N48.8874; E106.2668	NS	E	10E	270	80	N80E	S10E	55S	350	35
N48.8537; E106.3439	N40W	S50W	30S	50	60	–	–	–	–	–
N48.8537; E106.3439	NS	W	20W	90	70	–	–	–	–	–
N48.8538; E106.3439	NS	W	35W	90	55	N70W	S20W	44S	20	46
N48.8538; E106.3439	N45W	S45W	30S	45	60	N25W	S65W	55S	65	35
N48.8462; E106.3455	N40E	S50E	20S	310	70	N20E	S70E	25S	290	65
N48.8462; E106.3455	N70W	S20W	15S	20	75	–	–	–	–	–
N48.8528; E106.3474[c]	N50E	S40E	15S	320	75	N60W	S30W	30S	30	60
N48.8525; E106.3462	N30W	S60W	10S	60	80	N40E	S50E	30S	310	60
N48.8519; E106.3473	N40W	S50W	20S	50	70	–	–	–	–	–
N48.8519; E106.3473	N60W	S30W	15S	30	75	–	–	–	–	–
N48.8519; E106.3473	NS	W	30W	90	60	–	–	–	–	–
N48.8519; E106.3473	NS	W	10W	90	80	–	–	–	–	–
N48.8514; E106.3474	N40W	S50W	10S	50	80	N60W	S30W	50S	30	40
N48.8514; E106.3474	NS	E	20E	270	70	N25E	S65E	30S	295	60
N48.8510; E106.3476[d]	NS	W	25W	90	65	N10W	S80W	45S	80	45
N48.8553; E106.3515	N10E	N80W	10W	100	80	N20E	S70E	30S	290	70
N48.8539; E106.3561	N15W	S75W	35S	75	55	N10E	S80E	70S	280	20
Average Y–P plane (5)	N18W	S72W	9S	72	81	N76E	S14E	27S	346	63

The average Y–P planes were calculated using the InnStereo beta.7 (Schönberg and Pasotti 2016)

[a, b, c, d, e]Locations of the rock outcrop shown in Figs. 6a–d and 7a–d, respectively

younger NW-trending faults are recognized in the central and eastern part of the study area. These high-angle or vertical faults cut both the non-foliated and foliated cataclasite near Mt. Sevsüül and Mt. Zürüü (Fig. 2a).

Summarizing the above observations of rock structure: the bedding planes of the Haraa Group chiefly form a complex fold structure (Fig. 2c); the rocks of Ulaan Öndör Formation have NE-trending, NW dipping bedding planes (Fig. 2c); and the rocks of Örmögtei Formation form an open syncline fold (Fig. 2a, c). We first discovered a low-angle, southward-dipping thrust in this area, which has a top-to-the-north shearing (Fig. 8b, c). The thrust clearly cuts the Haraa Group, the granitic rocks, and the Ulaan Öndör Formation, with the exception of the Örmögtei Formation (Fig. 2a, b).

Age of the granitic rocks

As a result of the BSE and CL examination, a total of 124 zircon grains, with an exposure of more than 40 μm in diameter on the epoxy resin, were chosen for analysis from samples #12Hr1601 (equigranular granite), #11Hr54 (porphyritic granite), and 12Hr1011 (porphyritic rhyolite). Of these, 16 grains were ablated twice at the core and rim. Data were obtained from a total of 140 spots (Table 2) and plotted in a Concordia diagram using the Isoplot 3.75 software (Ludwig 2012). A total of 77 age data points were excluded from examination for various reasons (e.g., less than 0.05 Concordia age probability, or ages with an error of >100 Ma). The remaining 63 data points were used in this study and plotted on a weighted mean diagram (Fig. 10a–c). It is generally accepted that zircon grains with a high Th/U ratio (>0.2) are of magmatic origin, whereas those with a low Th/U ratio (<0.1) have undergone a secondary process, such as metamorphism and hydrothermal alteration (Hartmann et al. 2000; Hartmann and Santos 2004). The zircon samples in the present study, showing a high Th/U ratio (0.21–0.79), can thus be considered magmatic in origin (Table 2).

Sample #12Hr1601

This sample was collected from non-deformed equigranular granite (Fig. 2a). It is coarse-grained and holocrystalline dominated by microcline, plagioclase, hornblende, and biotite with minor zircon. The zircon grains of the equigranular granite are mostly light brown, subhedral to euhedral, semi-transparent, and up to 200 μm in length along their major axis. Most zircons have a few inclusions and cracks and yield dark unzoned CL images (e.g., Fig. 9a; Grain number 46 or G#46).

The Th/U ratio is 0.21–0.5 (Table 2). The ages from 31 concordant analyses ranging from 561 to 480 Ma (Fig. 10a) were grouped at 540.9 ± 8 Ma (10 grains, MSWD = 4.9, probability = 0.026) and 498.3 ± 3.3 Ma (21 grains, MSWD = 0.43, probability = 0.51). The older ages (~540 Ma) are likely to have been obtained from inherited cores within the zircon samples. The younger ages (~498 Ma) are likely to indicate the age of the magmatic event of the equigranular granite (Fig. 10a; Table 2).

Sample #11Hr54

This sample was taken from fractured porphyritic granite near the thrust (Fig. 2a). It is coarse-grained and holo- to hypocrystalline dominated by quartz, K-feldspar, and plagioclase with minor sphene, zircon, and opaque minerals. The zircons from this sample are yellow to colorless, transparent, euhedral to subhedral, up to 150 μm in length along their major axis, and have a length-to-width ratio of 1:2 (Fig. 9b). The zircons have irregular cracks and commonly

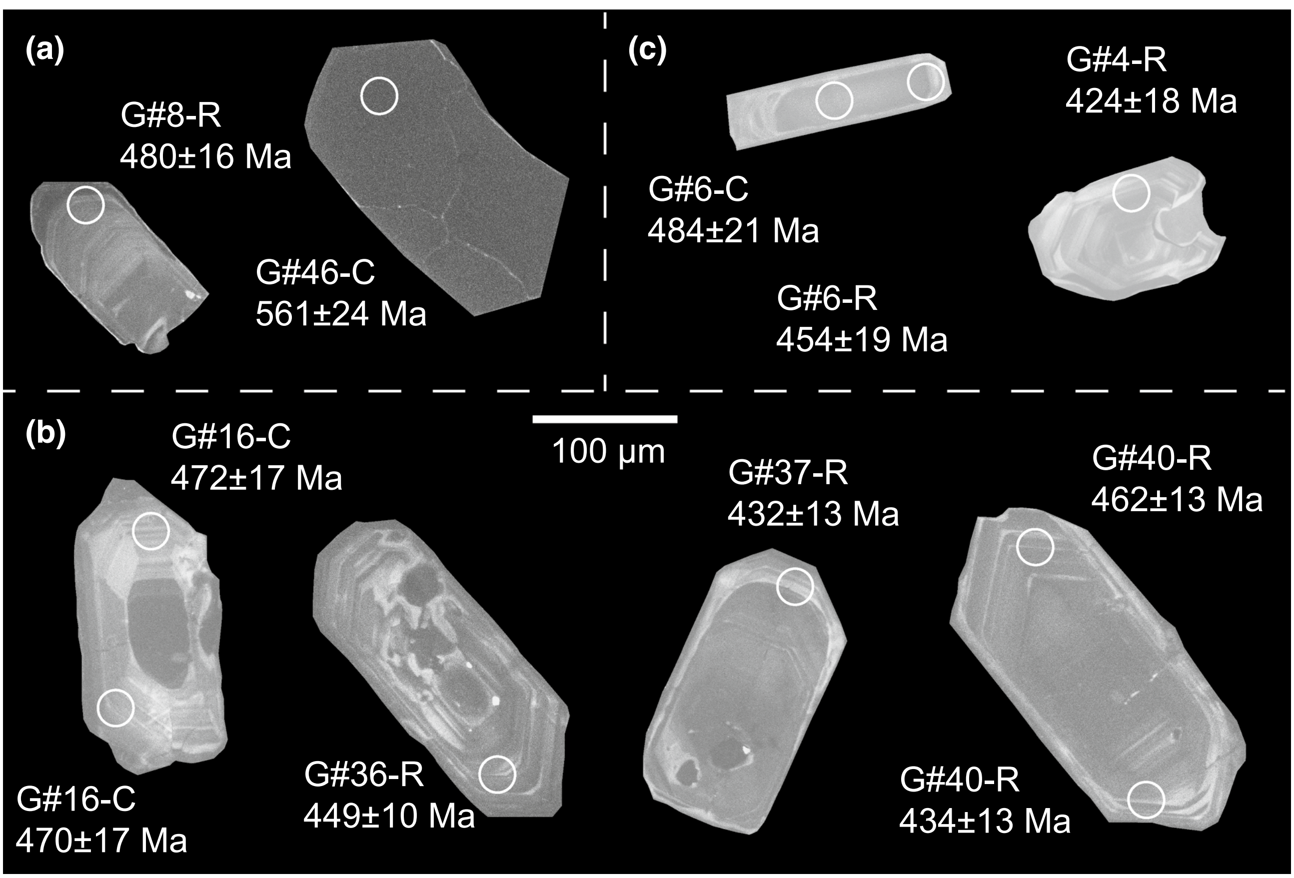

Fig. 9 Representative cathodoluminescence (CL) images of zircon grains from dated granitic rocks. Zircons from sample **a** #12Hr1601 (non-deformed equigranular granite), **b** #11Hr54 (fractured porphyritic granite), and **c** #12Hr1011 (a clast in the cataclasite derived from the porphyritic rhyolite). The locations of the analytical spots (C core and R rim) are shown as *circles* together with grain numbers (G#) and Concordia ages (in Ma). Diameter of analytical slot is 25 micrometer, and *white scale* denotes 100 μm. The analytical results refer to Table 2

Table 2 Analytical results of LA–ICP–MS U-Pb dating for granitic rock from the Züünharaa area

Rock, sample #, sample location, and total spot	Grain number and slot location	Th/U	Raw ratios				Apparent ages (Ma)								206Pbc[a] (%)	Concordia age (Ma)			
			207Pb/206Pb	Error (±2σ)	206Pb/238U	Error (±2σ)	207Pb/235U	Error (±2σ)	207Pb-206Pb age	Error (±2σ)	238U-206Pb age	Error (±2σ)	235U-207Pb age	Error (±2σ)		Conc. age (Ma)	Error (±2σ)	MSWD	Probability
(a) Equigranular granite, #12Hr1601, N48°53′43.8″, E106°37′36.2″, $n=31$	#1-C	0.47	0.0582	0.0023	0.0886	0.0030	0.7109	0.0370	537	21	545.3	28.4	547.3	18.3	0.14	547	17	0.06	0.81
	#2-C	0.34	0.0590	0.0024	0.0821	0.0028	0.6681	0.0356	568	23	519.5	27.7	508.7	17.1	0.27	510	16	1.60	0.20
	#3-C	0.32	0.0574	0.0023	0.0788	0.0026	0.6234	0.0328	507	21	492.0	25.9	488.9	16.4	0.04	489	16	0.15	0.70
	#4-C	0.29	0.0568	0.0023	0.0808	0.0027	0.6328	0.0336	485	20	497.8	26.5	500.8	16.8	0.00	500	16	0.12	0.73
	#7-C	0.25	0.0569	0.0023	0.0826	0.0028	0.6486	0.0342	489	20	507.6	26.7	511.8	17.2	0.10	511	16	0.26	0.61
	#8-R	0.34	0.0583	0.0027	0.0771	0.0027	0.6200	0.0356	542	25	489.8	28.1	478.9	16.8	0.31	480	16	1.50	0.22
	#9-C	0.34	0.0573	0.0009	0.0805	0.0027	0.6358	0.0233	502	7	499.7	18.3	499.3	16.7	0.09	500	14	0.01	0.92
	#11-C	0.39	0.0597	0.0019	0.0854	0.0038	0.7025	0.0383	592	19	540.3	29.4	528.3	23.2	0.43	533	21	2.90	0.09
	#20-R	0.21	0.0571	0.0018	0.0821	0.0032	0.6470	0.0327	497	16	506.6	25.6	508.9	19.9	0.00	508	18	0.12	0.73
	#23-C	0.38	0.0564	0.0017	0.0818	0.0032	0.6361	0.0316	468	14	499.9	24.9	507.0	19.8	0.04	504	18	1.20	0.27
	#25-C	0.46	0.0573	0.0017	0.0921	0.0036	0.7273	0.0357	503	15	554.9	27.2	567.9	22.1	0.05	561	20	3.60	0.06
	#27-C	0.25	0.0581	0.0018	0.0834	0.0033	0.6677	0.0335	532	17	519.3	26.0	516.5	20.1	0.23	518	19	0.18	0.67
	#28-C	0.30	0.0567	0.0014	0.0797	0.0023	0.6226	0.0239	479	12	491.4	18.9	494.2	14.4	0.23	493	13	0.29	0.59
	#32-C	0.31	0.0567	0.0015	0.0803	0.0023	0.6278	0.0248	481	13	494.7	19.5	497.8	14.6	0.00	497	14	0.33	0.56
	#33-C	0.49	0.0573	0.0014	0.0853	0.0025	0.6737	0.0253	503	12	522.9	19.7	527.6	15.4	0.00	526	14	0.81	0.36
	#34-R	0.34	0.0565	0.0014	0.0820	0.0024	0.6391	0.0248	473	12	501.7	19.5	508.3	14.8	0.00	506	14	1.50	0.21
	#37-C	0.31	0.0574	0.0017	0.0890	0.0021	0.7039	0.0270	507	15	541.1	20.8	549.4	13.1	0.04	548	12	1.60	0.20
	#38-C	0.43	0.0573	0.0017	0.0889	0.0021	0.7020	0.0266	504	15	539.9	20.4	548.7	13.0	0.17	547	12	1.90	0.16
	#39-R	0.38	0.0588	0.0017	0.0801	0.0019	0.6487	0.0244	559	16	507.7	19.1	496.5	11.8	0.39	498	11	3.60	0.06
	#40-R	0.34	0.0557	0.0017	0.0795	0.0019	0.6105	0.0239	440	14	483.9	18.9	493.4	11.8	0.00	492	11	2.50	0.12
	#45-R	0.36	0.0575	0.0018	0.0803	0.0019	0.6370	0.0250	511	16	500.4	19.6	498.2	11.9	0.00	498	11	0.13	0.72
	#46-C	0.37	0.0577	0.0022	0.0917	0.0042	0.7300	0.0435	520	20	556.5	33.2	565.5	26.2	0.00	561	24	1.13	0.29
	#50-C	0.35	0.0575	0.0021	0.0802	0.0037	0.6356	0.0377	511	19	499.6	29.7	497.1	23.0	0.09	498	21	0.10	0.75
	#51-C	0.50	0.0576	0.0021	0.0886	0.0041	0.7037	0.0418	516	19	541.0	32.2	547.2	25.3	0.11	544	23	0.56	0.45
	#53-C	0.27	0.0566	0.0021	0.0852	0.0039	0.6644	0.0395	475	18	517.3	30.7	527.1	24.4	0.08	523	22	1.50	0.22
	#54-C	0.32	0.0579	0.0022	0.0820	0.0038	0.6549	0.0392	527	20	511.5	30.6	508.0	23.5	0.01	509	22	0.19	0.66
	#55-R	0.31	0.0556	0.0022	0.0828	0.0030	0.6347	0.0341	436	17	499.0	26.8	512.9	18.6	0.04	509	17	3.00	0.08
	#56-R	0.35	0.0558	0.0022	0.0807	0.0029	0.6201	0.0336	444	18	489.9	26.5	500.0	18.1	0.00	498	17	1.60	0.21
	#57-R	0.27	0.0564	0.0022	0.0794	0.0029	0.6171	0.0330	468	18	488.0	26.1	492.4	17.8	0.05	491	17	0.31	0.58
	#61-R	0.33	0.0584	0.0023	0.0818	0.0030	0.6590	0.0351	545	21	514.0	27.3	507.1	18.4	0.52	509	17	0.73	0.39
	#62-R	0.37	0.0564	0.0023	0.0776	0.0028	0.6036	0.0329	468	19	479.5	26.1	482.0	17.5	0.09	482	17	0.10	0.75

Table 2 (continued)

Rock, sample #, sample location, and total spot	Grain number and slot location	Th/U	Raw ratios				Apparent ages (Ma)								206Pbc[a] (%)	Concordia age (Ma)			
			207Pb/206Pb	Error (±2σ)	206Pb/238U	Error (±2σ)	207Pb/235U	Error (±2σ)	207Pb-206Pb age	Error (±2σ)	238U-206Pb age	Error (±2σ)	235U-207Pb age	Error (±2σ)		Conc. age (Ma)	Error (±2σ)	MSWD	Probability
(b) Porphyritic granite, #11Hr54, N48°55′ 21.1″, E106°31′13.3″, $n=23$	#1-C	0.58	0.0572	0.0024	0.0796	0.0020	0.6281	0.0312	500	21.3	493.9	12.6	494.9	24.6	0.40	494	12	0.01	0.91
	#6-R	0.45	0.0550	0.0030	0.0735	0.0019	0.5582	0.0334	414	22.2	457.5	12.1	450.3	26.9	n.d	457	12	0.54	0.46
	#7-C	0.42	0.0549	0.0032	0.0777	0.0021	0.5889	0.0375	411	23.8	482.6	12.9	470.2	30.0	n.d	482	12	1.30	0.25
	#9-R	0.53	0.0566	0.0026	0.0748	0.0020	0.5837	0.0309	477	22.0	464.8	12.1	466.8	24.7	0.02	465	12	0.05	0.82
	#11-R	0.47	0.0582	0.0029	0.0692	0.0024	0.5555	0.0336	539	26.6	431.3	15.1	448.6	27.1	n.d	433	15	3.60	0.06
	#13-R	0.44	0.0605	0.0049	0.0742	0.0028	0.6195	0.0557	623	50.9	461.6	17.4	489.5	44.0	n.d	462	17	3.00	0.08
	#14-C	0.54	0.0589	0.0023	0.0788	0.0027	0.6405	0.0331	565	21.8	489.0	16.8	502.6	26.0	0.35	491	16	3.00	0.08
	#16-C	0.46	0.0591	0.0043	0.0755	0.0028	0.6154	0.0504	572	41.8	469.1	17.3	486.9	39.9	n.d	470	17	1.60	0.21
	#16-C	0.47	0.0595	0.0047	0.0759	0.0028	0.6227	0.0540	586	45.9	471.7	17.6	491.6	42.6	n.d	472	17	1.70	0.20
	#19-R	0.37	0.0567	0.0032	0.0720	0.0012	0.5627	0.0336	479	27.4	448.3	7.8	453.2	27.0	n.d	448	8	0.23	0.63
	#25-C	0.45	0.0554	0.0026	0.0774	0.0012	0.5908	0.0293	427	20.1	480.6	7.5	471.4	23.3	1.02	480	7	1.08	0.30
	#26-C	0.39	0.0573	0.0030	0.0768	0.0013	0.6065	0.0328	503	25.9	476.9	7.8	481.3	26.1	0.53	477	8	0.20	0.65
	#28-R	0.40	0.0576	0.0031	0.0743	0.0017	0.5897	0.0340	515	27.4	461.7	10.4	470.6	27.2	n.d	462	10	0.78	0.38
	#31-R	0.48	0.0580	0.0032	0.0735	0.0017	0.5878	0.0355	531	29.7	457.1	10.4	469.5	28.4	n.d	458	10	1.40	0.25
	#32-R	0.46	0.0550	0.0028	0.0755	0.0017	0.5724	0.0313	413	20.7	469.1	10.3	459.5	25.1	n.d	469	10	1.05	0.30
	#36-R	0.50	0.0552	0.0030	0.0721	0.0016	0.5487	0.0324	419	22.9	449.0	10.1	444.1	26.2	n.d	449	10	0.25	0.62
	#37-R	0.38	0.0569	0.0028	0.0693	0.0021	0.5436	0.0310	488	23.6	431.8	13.0	440.8	25.1	0.85	432	13	1.05	0.31
	#38-R	0.49	0.0572	0.0026	0.0695	0.0021	0.5483	0.0300	502	23.0	432.9	12.9	443.8	24.3	1.51	434	12	1.70	0.19
	#40-R	0.42	0.0588	0.0028	0.0741	0.0022	0.6013	0.0339	562	26.8	460.9	13.9	478.1	26.9	0.09	462	13	3.50	0.06
	#40-R	0.41	0.0532	0.0030	0.0698	0.0021	0.5116	0.0332	336	19.2	434.9	13.3	419.5	27.2	1.19	434	13	2.50	0.12
	#44-R	0.49	0.0575	0.0026	0.0729	0.0022	0.5780	0.0316	512	23.4	453.5	13.5	463.2	25.3	0.05	454	13	1.30	0.26
	#47-R	0.47	0.0566	0.0033	0.0732	0.0020	0.5706	0.0366	475	27.5	455.2	12.6	458.4	29.4	0.27	455	12	0.09	0.77
	#59-C	0.48	0.0588	0.0036	0.0777	0.0021	0.6294	0.0423	559	34.4	482.2	12.9	495.7	33.3	0.03	483	12	1.20	0.27
(c) Porphyritic rhyolite, *#12Hr1011*, N48°54′26.6″, E106°13′50.3″, $n=9$	#4-R	0.50	0.0566	0.0036	0.0679	0.0031	0.5302	0.0412	478	30.2	423.5	19.1	431.9	33.6	0.72	424	18	0.56	0.46
	#5-C	0.42	0.0542	0.0044	0.0850	0.0027	0.6346	0.0557	379	30.9	525.7	16.9	499.0	43.8	n.d	524	16	2.80	0.10
	#5-R	0.44	0.0588	0.0036	0.0722	0.0022	0.5855	0.0394	562	33.9	449.1	13.4	467.9	31.5	0.02	450	13	2.70	0.10
	#6-C	0.40	0.0563	0.0047	0.0781	0.0036	0.6061	0.0576	464	38.7	484.7	22.2	481.1	45.7	3.98	484	21	0.05	0.82
	#6-R	0.79	0.0569	0.0036	0.0728	0.0032	0.5712	0.0436	487	30.5	453.2	19.9	458.7	35.0	0.42	454	19	0.23	0.63
	#7-R	0.58	0.0584	0.0040	0.0734	0.0033	0.5908	0.0485	544	37.5	456.7	20.3	471.4	38.7	1.34	458	19	1.20	0.26
	#8-R	0.35	0.0566	0.0043	0.0726	0.0033	0.5667	0.0500	477	36.2	451.7	20.3	455.8	40.2	0.57	452	20	0.09	0.77
	#9-R	0.39	0.0568	0.0045	0.0738	0.0034	0.5780	0.0530	483	38.5	459.2	20.8	463.1	42.4	n.d	460	20	0.07	0.79
	#9-R	0.49	0.0594	0.0044	0.0730	0.0033	0.5983	0.0516	583	42.9	454.4	20.4	476.1	41.1	0.78	456	20	2.30	0.13

Concordia age, MSWD, and Probability were calculated using the Isoplot 3.75 software (Ludwig 2012)

n.d. no detection of 204Pb, *C* core, *R* rim

[a]Percentage of 206Pb contributed by common Pb on the basis of 204Pb. Value of common Pb was assumed by Stacey and Kramers (1975) model

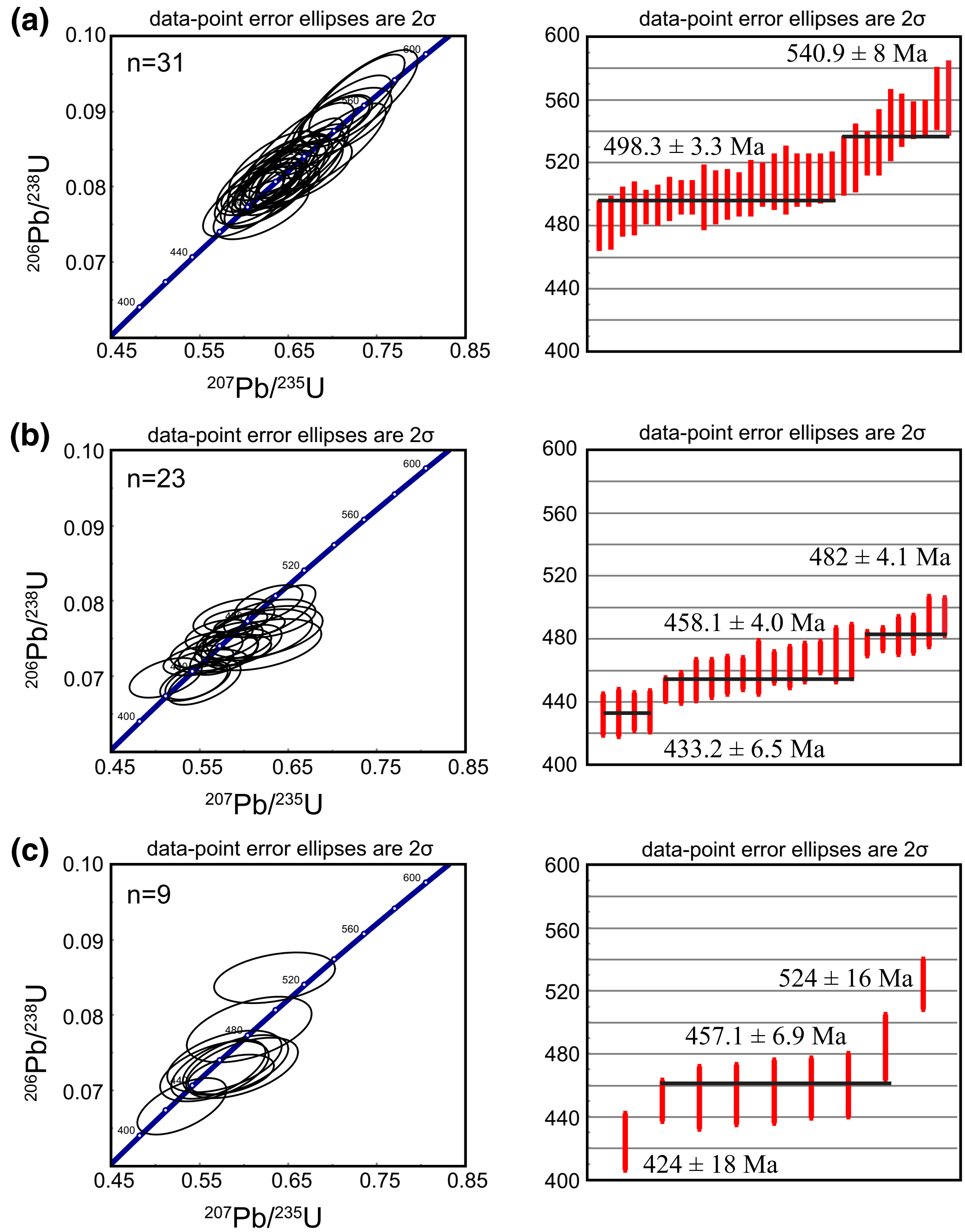

Fig. 10 U-Pb Concordia and mean weighted diagrams of zircon grains from granitic rocks. **a** Equigranular granite, **b** porphyritic granite, and **c** porphyritic rhyolite. The analytical results refer to Table 2. *n* A total number of analytical spot. The error ellipses in the Concordia plots are 2σ

include apatite needles (e.g., Fig. 9b, G#36 and G#37). Some zircon grains show inherited cores with concentric oscillatory zoning in their CL images (Fig. 9b, G#16).

The Th/U ratio is 0.39–0.58 (Table 2). The ages from 23 concordant analyses ranging from 494 to 432 Ma (Fig. 10b) are grouped at 482 ± 4.1 Ma (6 grains, MSWD = 0.5, probability = 0.48), 458.1 ± 4 Ma (13 grains, MSWD = 3.8, probability = 0.05) and 433.2 ± 6.5 Ma (4 grains, MSWD = 2.1, probability = 0.15). The oldest group was mostly obtained from the core of the grain (Fig. 9b, G#16), whereas the youngest grain, 432 ± 13 Ma (MSWD = 1.05, probability = 0.31), was from a rim location (Fig. 9b, G#37-R; Table 2). Therefore, the youngest group age of ca. 433.2 ± 6.5 Ma is considered to be of the same age as the porphyritic granite magmatism (Fig. 10b).

Sample 12Hr1011

This sample is a clast in the cataclasite of the thrust. It is fine-grained porphyritic rhyolite with phenocrysts of quartz, K-feldspar, and plagioclase. The zircons from this sample are commonly needle-shaped or acicular, euhedral, transparent, and range from 50 to 150 μm in length along their major axis. Fewer cracks and apatite needles are included. Most grains show concentric oscillatory zoning in their CL images (e.g., Fig. 9c).

The Th/U ratio is 0.35–0.79 (Table 2). The ages from nine concordant analyses ranging from 524 to 424 Ma (Fig. 10c) are grouped at 457.1 ± 6.9 Ma (7 grains, MSWD = 4.2, probability = 0.04). The youngest age, 424 ± 18 Ma (one grain, MSWD = 0.56, probability = 0.46), was obtained from an oscillatory zoned rim (Fig. 9c, G#4-R), and the 484 ± 21 Ma and 454 ± 19 Ma ages were obtained from the core and rim of a single grain of zircon, respectively (Fig. 9c, G#6-C and G#6-R). The older (~524 Ma) and younger (~450–420 Ma) ages can, therefore, be interpreted as having been inherited which were extracted from crustal materials and magmatic porphyritic rhyolite.

Shortly, the U-Pb ages of 561–480, 492–432, and 524–424 Ma are yielded from zircons, which extracted from samples of the equigranular granite (#12Hr1601), porphyritic granite (#11Hr54), and porphyritic rhyolite (#12Hr1011), respectively. These U-Pb ages correspond to the Ediacaran to Late Silurian.

Discussion

Timing of the low-angle southward-dipping thrusting in the Züünharaa area

The low-angle southward-dipping thrust in this area clearly cuts the Haraa Group, the porphyritic granite–rhyolite, and the Ulaan Öndör Formation, with the exception the Örmögtei Formation. The granitic rocks had U-Pb ages ranging from 561 to 424 Ma (Figs. 2, 10) and coincide with the U-Pb ages of the Boroogol plutonic rock complex dated at 460–440 Ma (e.g., Kröner et al. 2007; Hou et al. 2010).

Magmatic zircon from the porphyritic granite–rhyolite clast in the cataclasite shows ages of ~450–420 Ma, and detrital zircons of ~450 Ma were reported from the Haraa Group (Bussien et al. 2011; Kröner et al. 2007; Kelty et al. 2008). This suggests that the low-angle south-dipping thrust occurred after the formation of the Haraa Group and the intrusion of the porphyritic granite–rhyolite into the Haraa Group. The tuff breccia of the Ulaan Öndör Formation, which contains abundant clasts of porphyritic granite–rhyolite and covers the Haraa Group and granitic rocks, is cut by the southward-dipping thrust. Yet, the clastic rocks Visean Örmögtei Formation were not affected by shearing. The thrusting can thus be considered to have occurred between the Silurian and the Visean.

Distribution of the low-angle southward-dipping thrust and regional correlation of the Haraa terrane

Several studies have reported low-angle faults similar to the low-angle southward-dipping thrust from the Haraa terrane (L.2–L.4, Fig. 1b, e.g., Tomur et al. 1994; Purevsuren and Narantsetseg 1998; Dejidmaa 2003; Tovuudorj 2003; Altanzul and Baasandolgor 2014). The meta-sandstone of the Cambrian–Early Ordovician Haraa Group thrusts over Middle–Late Ordovician porphyritic rhyolite at Zuunmod area, 30 km southeast of the study area (L.2, Fig. 1b; Altanzul and Baasandolgor 2014). The thrust plane strikes N 20° E and gently dips southward (Altanzul and Baasandolgor 2014). Dejidmaa (2003) reports that a sub-horizontal top-to-the-north fault cuts volcaniclastic rocks of the Devonian Ulaan Öndör Formations at Bayangol area, 40 km west of the study area (L.3, Fig. 1b). Kelty et al. (2008) suggested that the Carboniferous Örmögtei Formation is exposed as a tectonic window below the Cambrian–Early Ordovician Haraa Group in the Zaamar area, 150 km southwest of the study area (L.4, Fig. 1b). Although details of the ages of the faults still remain unknown, they are likely to originate in the Late Paleozoic based on the fact that it is generally hard to recognize low-angle faults in the Triassic/Jurassic granites distributed throughout the Haraa terrane (e.g., Tomurtogoo et al. 1998).

Late Paleozoic low-angle southward-dipping thrusts are also recognized in the SB belt in North Mongolia and West Transbaikal, northwest of HD belt (Fig. 1b) (e.g., Zorin 1999; Ruzhentsev et al. 2006, 2007, 2012; Buslov et al. 2009; Ryabinin et al. 2011; Zhimulev et al. 2011). Buslov et al. (2009) and Zhimulev et al. (2011) reported that the Neoproterozoic–Cambrian formations overthrust upon the Middle Ordovician Tunka granite and the Late Devonian–Early Carboniferous Sagan-Sair Formation with an E–W trending plane and dipping less than 30° southward in the Tunka area (L.4; Fig. 1b).

The minerals (such as amphibole, biotite and muscovite) at the bottom of the tectonic sheet of the Neoproterozoic-Cambrian formations (dated at an U-Pb age of 2–1.7 Ga; Zhimulev et al. 2010) yield an Ar–Ar age of 316–310 Ma, which correspond to the Late Carboniferous (e.g., Buslov et al. 2009; Ryabinin et al. 2011; Zhimulev et al. 2011). Ryabinin et al. (2011) and Zhimulev et al. (2011) interpreted this isotopic age as the timing of the low-angle southward-dipping thrusts.

Several examples of Late Paleozoic low-angle south-dipping thrusts can be seen in the Ul'zutui, Oldynda, Kydzhimit areas of the Eravna terrane, SB belt (L.5, Fig. 1b). The andesite dated at 310 Ma and felsite dated at 297 Ma occur as a series of tectonic sheets alternating with slices of Lower Paleozoic rocks along low-angle south-dipping plane in the Ul'zutui, Oldynda, and Kydzhimit areas of the Eravna terrane (Ruzhentsev et al. 2012). Another example of Late Paleozoic thrust is found in the Bagdarin area of the Ikat terrane (L.6, Fig. 1b). The Neoproterozoic-to-Middle Paleozoic formation thrusts onto the Late Devonian–Early Carboniferous Bagdarin Formation along low-angle south-dipping planes in this area (Ruzhentsev et al. 2007, 2012). The Usoi granitic rocks of the Angara-Vitim batholith (dated as 288 ± 2 Ma) cut both the hanging-wall and footwall of the low-angle south-dipping thrust in the Bagdarin area (Ruzhentsev et al. 2007; Mazukabsov et al. 2010). It can thus be concluded that the thrusts in the Ul'zutui, Oldynda, Kydzhimit, and Bagdarin areas were formed after the Early Carboniferous and before the Early Permian periods.

The above observations, i.e., L.1–L.6 (Fig. 1b), make it clear that the Late Paleozoic low-angle southward-dipping thrust can generally be recognized in both the HD and SB belts. It should be noted that Proterozoic–Early Paleozoic sedimentary rocks are intruded by Cambrian–Ordovician granitic rocks and unconformably overlain by Late Paleozoic sedimentary rocks in the SB belt (e.g., Parfenov et al. 2009; Buslov et al. 2013). In the Haraa terrane of the HD belt, however, Cambrian–Lower Ordovician sedimentary rocks are intruded by Cambrian–Silurian granitic rocks and are unconformably overlain by Devonian–Carboniferous volcaniclastic and clastic rocks (e.g., Tomurtogoo et al. 1998; Tomurtogoo 2012). Thus, the general Paleozoic stratigraphy of this terrane is substantially the same as that of the SB belt. It is generally accepted that the SB belt is a collage of blocks with granitic batholiths that were accreted to the Siberian craton during the Early Paleozoic (e.g., Parfenov et al. 2009), and which behaved as a part of the continent during the Paleozoic. Badarch (2005) expressed that the northwest of the Haraa terrane is the Precambrian continental basement rock beneath the Permian–Triassic superimposed volcanic–plutonic rocks, which is connected with the SC in the North Mongolia–West Transbaikal region (Fig. 1b). Together with the observations discussed above, it follows that the existence of the Late Paleozoic low-angle southward-dipping thrust and the stratigraphic similarity in both the Haraa terrane and the SB belt seems to demonstrate that the Haraa terrane can be correlated to the SB belt as a part of the continent.

Tectonic implication of the low-angle southward-dipping thrust

The Haraa terrane is limited by the NE-trending Late Mesozoic Yeroogol sinistral strike-slip fault system (e.g., Tseden et al. 1992; Kotlyar et al. 1998; Altanzul and Delgertsogt 2012; Altanzul and Baasandolgor 2014) at its southern end, as well as by its contact with the Asralt Hairhan terrane of HD belt (Fig. 1b). The Asralt Hairhan terrane is considered to have a metamorphic affinity to the Ulaanbaatar terrane (Tomurtogoo 2012; Gordienko et al. 2012). The Ulaanbaatar terrane is a late Devonian–Early Carboniferous accretionary complex (Kurihara et al. 2009). Several authors (e.g., Zorin 1999; Dorjsuren et al. 2006; Kurihara et al. 2009; Bussien et al. 2011; Gordienko et al. 2012; Takeuchi et al. 2012; Hara et al. 2013; Purevjav and Roser 2013; Ruppen et al. 2013; Tsukada et al. 2013) have been studied the lithology, stratigraphy, geological structure, geochemistry, and age of the rocks in the Paleozoic accretionary complexes of the HD belt. Detrital zircons in the sandstone of the accretionary complex of the Ulaanbaatar terrane mostly yield U-Pb ages of ~350–320 Ma (e.g., Kröner et al. 2007; Kelty et al. 2008; Bussien et al. 2011; Hara et al. 2013). The rocks of the accretionary complex are unconformably overlain by formations yielding Carboniferous brachiopods (e.g., Minjin et al. 2006; Kurihara et al. 2009; Takeuchi et al. 2012), and it can thus be inferred from the ages of the detrital zircon and overlying formation that the clastic rocks of the accretionary complex should be assigned to the Carboniferous. The sandstones of the accretionary complex and overlying formation in the Ulaanbaatar terrane (Fig. 5a, b, e.g., Bussien et al. 2011; Hara et al. 2013; Suzuki et al. 2012) are located in the "Basement uplift" and "Volcanic arc" fields in the Q–F–Lt diagram (Dickinson et al. 1983), as is the coeval sandstone of the Örmögtei Formation in the Haraa terrane. The sandstone of the Örmögtei Formation includes detrital zircon, most of which yields an U-Pb age of ~360–330 Ma (Kröner et al. 2007; Kelty et al. 2008). The similarities in detrital zircon ages and sandstone compositions in the Carboniferous formations of the Haraa and Ulaanbaatar/Asralt Hairhan terranes likely suggest that the sandstones were formed in adjacent areas. That is, there existed a continental affinity between the Haraa terrane and accretionary complexes of the Ulaanbaatar/Asralt Hairhan terranes, and they were probably located close together during the Carboniferous.

Several studies have described southeast-verging composite folds and northward-dipping thrusts in the accretionary complexes of the Asralt Hairhan and Ulaanbaatar terranes (L.8, Fig. 1b, e.g., Kurihara et al. 2009; Gordienko et al. 2012; Nakane et al. 2012; Suzuki et al. 2012; Takeuchi et al. 2012). These have been interpreted as showing that the folds and thrusts in these terranes were formed in relation to northward subduction of the previous oceanic plate beneath the continental crust (e.g., Kurihara et al. 2009; Gordienko et al. 2012; Takeuchi et al. 2012; Ruppen et al. 2013). Kurihara et al. (2009) proposed that the accretion process may have taken place between the late Devonian and Early Carboniferous, and Hara et al. (2013) inferred the accretion age of the clastic rocks as Early Carboniferous, based on the U-Pb age of detrital zircon in the Ulaanbaatar terrane. Early Permian mafic-to-felsic dikes cut the folded clastic rocks of the accretionary complex of the Ulaanbaatar terrane (Khishigsuren et al. 2009). Hence, the southeast-verging folds and northward-dipping thrusts are considered to have been formed before the Early

Permian. In summary, Late Paleozoic southward-dipping thrusts are dominant in the Tunka, Ikat, and Eravna terranes of the SB belt and the Haraa terrane of the HD belt (L.1–L.7, Fig. 1b). In contrast, contemporaneous southeast-verging composite folds and northward-dipping thrusts have developed in the Asralt Hairhan and Ulaanbaatar terranes (L.8, Fig. 1b).

Simultaneously formed "doubly vergent (or bivergent; e.g., Willett et al. 1993; Storti et al. 2000; Naylor and Sinclair 2007; Mukherjee 2013b; Bose and Mukherjee 2015) asymmetric structures", similar to those present in the HD and SB belt, have been illustrated in the Alps, the Andes, and in other locations. For instance, the Taranaki Fault in the northern part of New Zealand is considered to be a back thrust antithetic to the Hikurangi margin subduction thrusts. The Taranaki Fault has accommodated at least 12–15 km of dip-slip displacement since the middle Eocene (~40–43 Ma) (e.g., Stern et al. 2006; Nicol et al. 2007; Stagpoole and Nicol 2008).

The doubly verging character of the Eastern Alps architecture is evident from the predominant criss–cross reflection pattern at ~10 km depth in a 150–220 km interval of a ~300 km seismic section (Gebrande et al. 2006), along which giant crustal wedges have been upthrust since the Miocene (Pfiffner et al. 2000). The southward- and northward-dipping thrusts are exposed at the Inn Valley and the Valsugana-Agordo areas in the Eastern Alps, respectively (Slejko et al. 1989).

Another example can be seen in France and Spain. The doubly vergent asymmetric structure characterizes a ~150-km-wide surface expression of the Hercynian basement, thin-skinned fold-thrust belts shown by the 250-km-long deep seismic survey (ECORS Pyrenees profile; Choukfoune 1989) from the Aquitaine basin to the Ebro basin of the Pyrenees (Sinclair et al. 2005). This structure is considered to have formed in the Pyrenees as a result of northward subduction of the Iberian plate beneath the East European craton during Late Cretaceous to early Miocene times (Roest and Srivastava 1991; Sinclair et al. 2005).

The Andes are sustained by large doubly vergent thrust systems (West Andean and East Andean Thrust) close to latitude 21°S (e.g., McQuarrie et al. 2005; Armijo et al. 2015). This is a result of the protracted processes of doubly vergent crustal shortening and thickening in the more than 600-km-wide regions of the high Andes-Altiplano plateau, since 50 Ma has been compressed between the rigid Marginal Block and the South America Plate (Armijo et al. 2015).

As shown in the above examples, the doubly vergent asymmetric structure is common in the plate convergence fields, i.e., subduction and collision zones. The oceanward-verging folds and thrusts are developed in accretionary complexes, whereas the landward-verging thrusts are formed on the continental side under the Alpine-type compressional orogen (e.g., Beaumont et al. 1996; Poblet and Lisle 2011) such as Alps and Himalaya (Mukherjee et al. 2013, 2015).

In the HD and SB belts, the area of southeastwardly-verging composite folds and northward-dipping thrusts (Asralt Hairhan and Ulaanbaatar terranes) exposes accretionary complexes. In contrast, the areas dominated by southward-dipping thrusts (Tunka, Ikat, Eravna, and Haraa terranes) are assigned to a part of the continent with Siberian craton. These contrasting structures suggest that there is a doubly vergent asymmetric structure in the North Mongolia–West Transbaikal region. However, the Permian–Triassic volcanic–plutonic rock complexes largely exposed in the areas between the Haraa terrane of the HD belt and the terranes of the SB belt, and the Late Paleozoic structure is obscure (Fig. 1b). The volcanic–plutonic rock complexes are interpreted to be the result of subduction-related

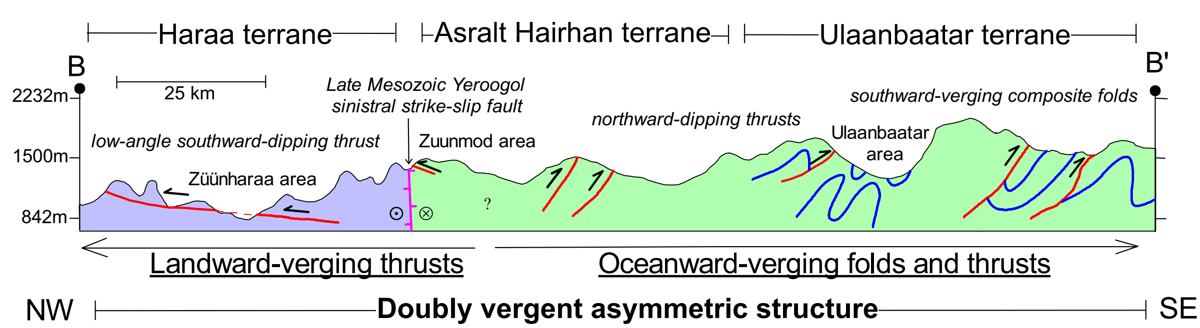

Fig. 11 Schematic section of the Late Paleozoic doubly vergent asymmetric structure in the HD belt. *Blue lines* are southward-verging composite folds of accretionary complexes in the Ulaanbaatar and Asralt Hairhan terranes. *Red lines* are south- and northward-dipping thrusts. The *vertical line* is the Mesozoic Yeroogol sinistral strike-slip fault. This schematic section is compiled by this study with previously published geological maps (e.g., Kurihara et al. 2009; Gordienko et al. 2012; Takeuchi et al. 2012; Altanzul and Baasandolgor 2014)

magmatic activity along the Paleozoic continental margin of the Siberian craton (e.g., Donskaya et al. 2013).

We show the schematic section of the doubly vergent asymmetric structure within the HD belt (Fig. 11) because of lack of Late Paleozoic structures in the Permian–Triassic superimposed volcanic–plutonic rock complexes (Fig. 1b). The Late Mesozoic Yeroogol sinistral strike-slip fault system marks the geological and structural boundary between the Haraa terrane and the Asralt Hairhan terrane of the HD belt (Figs. 1b, 11; e.g., Tseden et al. 1992; Kotlyar et al. 1998; Badarch et al. 2002; Tomurtogoo 2003, 2012). This fault cuts the Triassic/Jurassic granites which are distributed in both Haraa and Asralt Hairhan terrane (Tomurtogoo et al. 1998); displacement of fault is ~1 km in the Zuunmod area (L.2, Fig. 1b; Altanzul and Delgertsogt 2012). Altanzul and Baasandolgor (2014) inferred that the Mesozoic Yeroogol sinistral strike-slip fault cuts the low-angle south-dipping thrust at Zuunmod area (Fig. 11b). By contrast, Gordienko et al. (2012) mentioned that there were a few northward-dipping thrusts in south of the Zuunmod area. The facts with ~1 km displacement of the Mesozoic Yeroogol fault suggests that a symmetry of the doubly vergent asymmetric structure in the HD belt may possibly be found near the Zuunmod area (L.2, Figs. 1b, 11). It can be concluded that the doubly vergent asymmetric structure was formed before the Mesozoic Yeroogol sinistral strike-slip fault. Thus, to understand the geometry and formation time of the doubly vergent asymmetric structure in the HD belt, further detailed study is essential.

Finally, the Paleozoic continental margin (Tunka, Ikat, Eravna and Haraa terrane) and Paleozoic accretionary complexes (Ulaanbaatar/Asralt Hairhan terranes) exists in the SB and HD belts. They were located in proximity during the Carboniferous based on their similarities in geological background. The former area (Fig. 1b) corresponds to the area of "oceanward-verging folds and thrusts" and "landward-verging thrusts" (Fig. 11) of Alpine-type compressional orogen. The doubly vergent asymmetric structure in the former area was formed by the northward subduction process of the Mongol Okhotsk oceanic plate (e.g., Zorin 1999; Bussien et al. 2011; Donskaya et al. 2013), which was previously present between SC and NCP/TB (Fig. 1a) in Late Paleozoic period.

Acknowledgements We wish to thank Profs. Makoto Takeuchi and Hidekazu Yoshida at Nagoya University for helpful advice. We are indebted to Dr. Sersmaa Gonchigdorj and Associate Prof. Munkhtsetseg Oidov at the Mongolian University of Science and Technology for valuable discussion and comments. We thank Prof. Koshi Yamamoto, Mr. Setsuo Yogo, and Ms. Masumi Nozaki at Nagoya University, Dr. Yuji Orihashi at Tokyo University, and Mr. Yoshiyuki Kouchi at University of Toyama for their technical support on the LA–ICP–MS dating. We appreciated to Barbara Rybak-Ostrowska and an anonymous reviewer for constructive comments and suggestions. Special thanks go to Dr. Soumyajit Mukherjee for three rounds of critical review while handling this manuscript. Authors are very grateful to the Chief Editor: Wolf-Christian Dullo and the Managing Editor: Monika Dullo.

Open Access This article is distributed under the terms of the Creative Commons Attribution 4.0 International License (http://creativecommons.org/licenses/by/4.0/), which permits unrestricted use, distribution, and reproduction in any medium, provided you give appropriate credit to the original author(s) and the source, provide a link to the Creative Commons license, and indicate if changes were made.

References

Altanzul Ch, Baasandolgor L (2014) Structural features of the Gatsuurt gold deposit, Mongolia. Haiguulchin 50:169–182

Altanzul Ch, Delgertsogt B (2012) Gold mineralization feature and its origin in the Zuunmod district, Mongolia. Haiguulchin 46:155–165

Ariunchimeg Y (2011) Carboniferous system. In: Byamba J (ed) Geology and mineral resource of Mongolia, Book I. Soyombo printing, Ulaanbaatar, pp 271–334

Armijo R, Lacassin R, Coudurier-Curveur A, Carrizo D (2015) Coupled tectonic evolution of Andean orogeny and global climate. Earth Sci Rev 143:1–35. doi:10.1016/j.earscirev.2015.01.005

Babar MD, Kaplay RD, Mukherjee S, Kulkarni PS (2016) Evidence of the deformation of dykes from Central Deccan Volcanic Province, Aurangabad, Maharashtra, India. In: Mukherjee S, Misra AA, Calvès G, Nemčok M (ed) Tectonics of the Deccan Large Igneous Province: an introduction. Geological Society, London, Special Publications 445. doi:10.1144/SP445.13 **(in press)**

Badarch G (2005) Tectonic overview of Mongolia. Mong Geosci 27:1–7

Badarch G, Cunningham WD, Windley BF (2002) A new terrane subdivision for Mongolia: implication for the Phanerozoic crustal growth of Central Asia. J Asian Earth Sci 21:87–110

Bartlett WL, Friedman M, Logan JM (1981) Experimental folding and faulting of rocks under confining pressure. Tectonophysics 79:255–277

Beaumont C, Ellis S, Hamilton J, Fullsack P (1996) Mechanical model for subduction-collision tectonics of Alpine-type compressional orogens. Geology 24:675–678

Belichenko VG, Reznitskii LZ, Geletii NK, Barash IG (2003) Tuva–Mongolia terrane (in the context of microcontinents in the Paleoasian ocean). Russ Geol Geophys 6:531–541

Bose N, Mukherjee S (2015) Back structures (back-faults and backfolds) from collisional orogen: field findings from Lesser Himalaya, Sikkim, India. In: 30th Himalaya-Karakoram-Tibet Workshop, Wadia Institute of Himalayan Geology, 06–08 Oct, Dehradun, India, pp 13–14

Buchan C, Cunningham D, Windley BF, Tomurhuu D (2001) Structural and lithological characteristics of the Bayankhongor Ophiolite Zone, Central Mongolia. J Geol Soc 158(3):445–460

Bulgatov AN, Gordienko IV (1999) Terranes, synaccretionary, and postaccretionary complexes of the Transbaikalia and southeastern part of Eastern Sayn Regions, Siberia. In: Nokleberg WJ, Naumova VV, Kuzmin MI, Bounaeva TV (ed) Preliminary publications book 1 from project on mineral resources, metallogenesis, and tectonics of Northeast Asia U.S. Geological Survey Open-File Report 99–165, pp 1–9

Bulgatov AN, Gordienko IV (2014) Fold systems of the Sayan-Baikal mountain area. In: Petrov OV, Leonov YG, Pospelov II (eds)

Tectonics of Northern, Central and Eastern Asia. Explanatory Note to the Tectonic map of Northern–Central–Eastern Asia and Adjacent Areas at scale 1:2 500 000. –SPb.: VSEGEI Printing House, pp 53–58. http://ccgm.org/en/maps/172-tectonic-map-of-northern-central-and-eastern-asia-9785937612151.html

Buslov MM, Ryabinin AB, Zhimulev FI, Travin AV (2009) Manifestations of the Late Carboniferous and Early Permian stages of formation of nappe–fold structures in the southern framework of the Siberian platform (East Sayany, South Siberia). Dokl Earth Sci 428(7):1105–1108

Buslov MM, Geng H, Travin AV, Otgonbaatar D, Kulikova AV, Chen Ming, Stijn G, Semakov NN, Rubanova ES, Abildaeva MA, Voitishek EE, Trofimova DA (2013) Tectonics and geodynamics of Gorny Altai and adjacent structures of the Altai–Sayan folded area. Russ Geol Geophys 54(10):1250–1271

Bussien D, Gombojav N, Winkler W, Quadt A (2011) The Mongol-Okhotsk Belt in Mongolia - An appraisal of the geodynamic development by the study of sandstone provenance and detrital zircons. Tectonophysics 510:132–150

Chang Z, Vervoort JD, McClelland WC, Knaack C (2006) U-Pb dating zircon by LA-ICP-MS. Geochem Geophys Geosyst 7:Q05009. doi:10.1029/2005GC001100

Choukfoune P (1989) The ECORS Pyrenean deep seismic profile reflection data and the overall structure of an orogenic belt. Tectonics 8:23–39

Corfu F, Hanchar JM, Hoskin PWO, Kinny P (2003) Atlas of zircon texture. In: Hanchar JM, Hoskin PWO (eds) Zircon. Mineralogical Society of American and Geochemical Society, Reviews in Mineralogy and Geochemistry 53(1), pp 469–500. doi:10.2113/0530469

Dejidmaa G (2003) Geological sheet map M-48-XXXIV at the scale of 1:200,000 with brief legend description. Geological Information Center, Mineral Resource Authority of Mongolia. Ulaanbaatar. Report #5565, pp 1–17

Dickinson WR, Beard LS, Brakenridge GR, Erjavec JL, Ferguson RC, Inman KF (1983) Provenance of North American Phanerozoic sandstones in relation to tectonic setting. Geol Soc Am Bull 94(2):222–235

Donskaya TV, Gladkochub DP, Mazukabzov AM, Ivanov AV (2013) Late Paleozoic-Mesozoic subduction-related magmatism at the southern margin of the Siberian continent and the 150 million-year history of the Mongol-Okhotsk Ocean. J Asian Earth Sci 62:79–97

Dorjsuren B, Bujinlkham B, Minjin Ch, Tsukada K (2006) Geological setting of the Ulaanbaatar terrane in the Hangay-Hentey zone of the Devonian accretionary complex, central Mongolia. In: Tomurhuu D, Natal'in BA, Ariunchimeg Y, Khishigsuren S, Erdenesaikhan G (eds) Structural and Tectonic Correlation across the Central Asia Orogenic Collage: Implications for Continental Growth and Intracontinental Deformation (second international workshop and field excursions for IGC Project 480), abstract and excursion guidebook. Mongolian University of Science and Technology Press, Ulaanbaatar, pp 39–42

Enkin RJ, Yang Z, Chen Y, Courtillot V (1992) Paleomagnetic constrains on the geodynamic history of major blocks of China from the Permian to the Present. J Geophys Res 97(B10):13953–13989

Fritzell EH, Bull AL, Shephard GE (2016) Closure of the Mongol–Okhotsk Ocean: Insights from seismic tomography and numerical modelling. Earth Planet Sci Lett 445:1–12. doi:10.1016/j.epsl.2016.03.042

Gebrande H, Lüschen E, Bopp M, Bleibinhaus F, Lammerer B, Oncken O, Stiller M, Kummerow J, Kind R, Millahn K, Grassl H, Neubauer F, Bertelli L, Borrini D, Fantoni R, Pessina C, Sella S, Castellarin A, Nicolich R, Mazzotti A, Bernabini M (2006) First deep seismic reflection images of the Eastern Alps reveal giant crustal wedges and transcrustal ramps. Geophys Res Lett 29(10). doi:10.1029/2006GL026618

Gordienko IV (2001) Geodynamic evolution of the Central-Asian and Mongol-Okhotsk fold belts and formation of the endogenic deposits. Geosci J 5:233–241

Gordienko IV, Filimonov AV, Minina OR (2007) The Dzhida island arc system in the Paleoasian Ocean: structure and main stages of Vendian–Paleozoic geodynamic evolution. Russ Geol Geophys 48(1):91–106

Gordienko IV, Medvedev AY, Gornova MA, Tomurtogoo O, Goneger TA (2012) The Haraa Gol terrane in the western Hentiyn Mountains (northern Mongolia): geochemistry, geochronology, and geodynamics. Russ Geol Geophys 53:281–292

Hara H, Kurihara T, Tsukada K, Kon Y, Uchino T, Suzuki T, Takeuchi M, Nakane Y, Nuramkhaan M, Chuluun M (2013) Provenance and origins of a Late Paleozoic accretionary complex within the Khangai-Khentei belt in the Central Asian Orogenic Belt, central Mongolia. J Southeast Asian Earth Sci 75:141–157. doi:10.1016/j.jseaes.2013.07.019

Hartmann LA, Santos JOS (2004) Predominance of high Th/U, magmatic zircon in Brazilian shield sandstone. Geology 32:73–76

Hartmann LA, Leite JAD, Silva LC, Remus MVD, McNaughton NJ, Groves DI, Fletcher IR, Santos JOS, Vasconcellos MAZ (2000) Advances in SHRIMP geochronology and their impact on understanding the tectonic and metallogenic evolution of southern Brazil. Aust J Earth Sci 47:829–844

Henley RW, Ellis AJ (1983) Geothermal systems ancient and modern: a geochemical review. Earth Sci Rev 19:1–50

Horn I, Blanckenburg FV (2007) Investigation on elemental and isotopic fractionation during 196 nm femtosecond laser ablation multiple collector inductively coupled plasma mass spectrometry. Spectrochimica Acta B 62:410–422

Hou W, Nie F, Jiang S, Bai D, Liu Y, Yun F, Liu Y (2010) SHRIMP zircon U-Pb dating of ore-bearing granite in the boroo large-size gold deposit, Mongolia and its geological significance. Acta Geoscientica Sinica 31(3):331–342. http://en.cnki.com.cn/Article_en/CJFDTotal-DQXB201003009.htm

Iwano H, Oshihashi Y, Hirata T (2013) An interlaboratory evaluation of OD-3 zircon for use as a secondary U–Pb dating standard. Isl Arc 22:382–394. doi:10.1111/iar.12038

Jahn BM, Wu FY, Chen B (2000) Granitoids of the Central Asian orogenic belt and continental growth in the phanerozoic. Trans R Soc Edinburgh arth Sci 91:181–193

Kaplay RD, Babar MD, Mukherjee S, Kumar TV (2016) Morphotectonic expression of geological structures in eastern part of the South East Deccan Volcanic Province (around Nanded, Maharashtra, India). In: Mukherjee S, Misra AA, Calvès G, Nemčok M (ed) Tectonics of the Deccan Large Igneous Province: an introduction, vol 445. Geological Society, Special Publications, London. doi:10.1144/SP445.12 **(in press)**

Kelty T, Yin A, Dash B, Gehrels GE, Ribeiro AE (2008) Detrital-Zircon geochronology of Paleozoic sedimentary rocks in the Hangay-Hentey basin, north-central Mongolia: Implications for the tectonic evolution of the Mongol–Okhotsk Ocean in central Asia. Tectonophysics 451:290–311

Khishigsuren S, Otoh S, Munkhbat B, Ohto Y (2009) New age data and tectonic setting of igneous rocks in the Ulaanbaatar area. Mong Geosci 35:51–57

Kotlyar B, Drown T, Tungalag F, Gantsetseg O (1998) Two type of mineralization in the North Khentei gold tend. Mong Geosci 11:10–13

Kouchi Y, Orihashi Y, Obara H, Fujimoo T, Haruta Y, Yamamoto K (2015) Zircon U–Pb dating by 213 nm Nd: YAG laser ablation inductively coupled plasma mass spectrometry: optimization of the analytical condition to use NIST SRM 610 for Pb/U fractionation correction. Chikyukagaku (Geochemistry) 49:19–35. doi:10.14934/chikyukagaku.49.19

Kovalenko VI, Yarmolyuk VV, Kovach VP, Kotov AB, Kozakov IK, Salnikova EB, Larin AM (2004) Isotope provinces, mechanisms of generation and sources of the continental crust in the Central Asian mobile belt: geological and isotopic evidence. J Asian Earth Sci 23:605–627

Kravchinsky VA, Cogné JP, Harbert WP, Kuzmin MI (2002) Evolution of the Mongol-Okhotsk Ocean as constrained by new palaeomagnetic data from the Mongol-Okhotsk suture zone, Siberia. Geophys J Int 148:34–57

Kröner A, Windley BF, Badarch G, Tomurtogoo O, Hegner E, Jahn BM, Gruschka S, Khain EV, Demoux A, Wingate MTD (2007) Accretionary growth and crust-formation in the Central Asian Orogenic Belt and comparison with the Arabian-Nubian shield. In: Hatcher RD Jr, Carlson MP, McBride JH, Martínez Catalán JR (eds) 4-D Framework of Continental Crust: Geological Society of America Memoir 200, vol 200, pp 181–209. doi:10.1130/2007.1200(11)

Kurihara T, Tsukada K, Otoh S, Kashiwagi K, Minjin C, Dorjsuren B, Bujinlkham B, Sersmaa G, Manchuk N, Niwa M, Tokiwa T, Hikichi G, Kozuka T (2009) Upper Silurian and Devonian pelagic deep-water radiolarian chert from the Khangai–Khentei belt of Central Mongolia: evidence for Middle Paleozoic subduction–accretion activity in the Central Asian Orogenic Belt. J Asian Earth Sci 34:209–225

Kurimoto Ch, Tungalag F, Bayarmandal L, Ichinnorov N (1998) K-Ar ages of white micas from pelitic schists of the Bayanhongor area, west Mongolia. Bull Geol Surv Jpn 49(1):19–23

Ludwig KR (2012) User's Manual for Isoplot 3.75. A Geochronological Toolkit for Microsoft Excel. Berkeley Geochronology Center Special Publication No. 5, 75p

Mazukabsov AM, Donskaya TV, Gladkochub DP, Paderian IP (2010) The Late Paleozoic geodynamics of the West Transbaikalian segment of the Central Asian fold belt. Russ Geol Geophys 51(5):482–491

McQuarrie N, Horton BK, Zandt G, Beck S, DeCelles PG (2005) Lithospheric evolution of the Andean fold-thrust belt, Bolivia, and the origin of the central Andean plateau. Tectonophysics 399:15–37. doi:10.1016/j.tecto.2004.12.013

Minjin Ch, Tomurtogoo O, Dorjsuren B (2006) Devonian-Carboniferous accretionary complex of the Ulaanbaatar terrane. In: Tomurhuu D, Natal'in BA, Ariunchimeg Y, Khishigsuren S, Erdenesaikhan G (eds) Structural and tectonic correlation across the central asia orogenic collage: implications for continental growth and intracontinental deformation (second international workshop and field excursions for IGC Project 480), abstract and excursion guidebook. Mongolian University of Science and Technology Press, Ulaanbaatar, pp 100–106

Misra AA, Mukherjee S (2016) Dyke-brittle shear relationships in the Western Deccan Strike-slip Zone around Mumbai (Maharashtra, India). In: Mukherjee S, Misra AA, Calvès G, Nemčok M (ed) Tectonics of the Deccan large igneous province, vol 445. Geological Society, London, Special Publications. doi:10.1144/SP445.4 **(in press)**

Mukherjee S (2010a) Structures at Meso- and Micro-scales in the Sutlej section of the Higher Himalayan Shear Zone in Himalaya. e-Terra 7:1–27

Mukherjee S (2010b) Microstructures of the Zanskar Shear Zone. Earth Sci India 3 (1):9–27

Mukherjee S (2012) Tectonic implications and morphology of trapezoidal mica grains from the Sutlej section of the Higher Himalayan Shear Zone, Indian Himalaya. J Geol 120(5):575–590. doi:10.1086/666744

Mukherjee S (2013a) Deformation microstructures in rocks. Springer, Berlin

Mukherjee S (2013b) Higher Himalaya in the Bhagirathi section (NW Himalaya, India): its structures, backthrusts and extrusion mechanism by both channel flow and critical taper mechanisms. Int J Earth Sci (Geol Rundsch) 102(7):1851–1870. doi:10.1007/s00531-012-0861-5

Mukherjee S (2014) Atlas of shear zone structures in meso-scale. Springer, Cham

Mukherjee S (2015) Atlas of structural geology. Elsevier, Amsterdam

Mukherjee S (2017) Shear heating by translational brittle reverse faulting along a single, sharp and straight fault plane. J Earth Syst Sci 126(1). doi:10.1007/s12040-016-0788-5

Mukherjee S, Koyi HA (2010a) Higher Himalayan Shear Zone, Sutlej Section: structural geology and extrusion mechanism by various combinations of simple shear, pure shear and channel flow in shifting modes. Int J Earth Sci (Geol Rundsch) 99(6):1267–1303. doi:10.1007/s00531-009-0459-8

Mukherjee S, Koyi HA (2010b) Higher Himalayan Shear Zone, Zanskar Indian Himalaya: microstructural studies and extrusion mechanism by a combination of simple shear and channel flow. Int J Earth Sci (Geol Rundsch) 99(5):1083–1110. doi:10.1007/s00531-009-0447-z

Mukherjee S, Mulchrone KF (2013) Viscous dissipation pattern in incompressible Newtonian simple shear zones: an analytical model. Int J Earth Sci (Geol Rundsch) 102(4):1165–1170. doi:10.1007/s00531-013-0879-3

Mukherjee S, Mukherjee B, Thiede R (2013) Geosciences of the Himalaya–Karakoram–Tibet orogen. Int J Earth Sci (Geol Rundsch) 102(7):1757–1758. doi:10.1007/s00531-013-0934-0

Mukherjee S, Carosi R, van der Beek PA, Mukherjee BK, Robinson DM (2015) Tectonics of the Himalaya: an introduction. Geol Soc Lond Spec Publ 412:1–3. doi:10.1144/SP412.14

Mulchrone KF, Mukherjee S (2015) Shear senses and viscous dissipation of layered ductile simple shear zones. Pure Appl Geophys 172(10):2635–2642. doi:10.1007/s00024-015-1035-8

Mulchrone KF, Mukherjee S (2016) Kinematics and shear heat pattern of ductile simple shear zones with 'slip boundary condition'. Int J Earth Sci (Geol Rundsch) 105(3):1015–1020. doi:10.1007/s00531-015-1206-y

Nakane Y, Kurihara T, Nuramkhaan B, Nuramkhaan M, Takeuchi M, Tsukada K, Gonchigdorj S, Sodnom Kh (2012) Geological division of the rocks at southeast of Ulaanbaatar (Gachuurt-Nalaikh), central Mongolia. Bull Nagoya Univ Museum 28:19–26. http://www.num.nagoya-u.ac.jp/outline/report/pdf/028_02.pdf

Naylor M, Sinclair HD (2007) Punctuated thrust deformation in the context of doubly vergent thrust wedge: Implications for the localization of uplift and exhumation. Geology 35:559–562

Nicol A, Mazengarb C, Chanier F, Rait G, Uruski C, Wallace L (2007) Tectonic evolution of the active Hikurangi subduction margin, New Zealand, since the Oligocene. Tectonics 26:TC4002. doi:10.1029/2006TC002090

Okada H (1971) Classification of sandstone: analysis and proposal. J Geol 79:509–525

Orihashi Y, Nakai S, Hirata T (2008) U-Pb age determination for seven standard zircons using inductively coupled plasma-mass spectrometry coupled with frequency quintupled Nd-YAG (λ = 213 nm) laser ablation system: comparison with LA-ICP-MS zircon analyses with a NIST glass reference material. Resour Geol 58:101–123

Parfenov LM, Khanchuk AI, Badarch G, Berzin NA, Hwang DH, Miller RJ, Naumova VV, Nokleberg WJ, Ogasawara M, Prokopiev AV, Yan H (2004a) Generalized Northeast Asia geodynamics map. In: Nokleberg WJ et al. (eds) Digital files for Northeast Asia Geodynamics, Mineral Deposit Location, and Metallogenic Belt Maps, Stratigraphic Columns, Descriptions of Map Units, and Descriptions of Metallogenic Belts, US

Geological Survey Open-File Report 2004–1252, CD-ROM, at scale 1:15 000 000
Parfenov LM, Khanchuk AI, Badarch G, Berzin NA, Miller RJ, Naumova VV, Nokleberg WJ, Ogasawara M, Prokopiev AV, Yan H (2004b) Descriptions of overlap assemblages and tectonostratigraphic terranes, definitions, and methods for compilation for Northeast Asia geodynamics map. US Geological Survey, Open-File Report 2004–1252, CD-ROM, explanatory text
Parfenov LM, Badarch G, Berzin NA, Berzin NA, Khanchuk AI, Kuzmin MI, Nokleberg WJ, Prokopiev AV, Ogasawara M, Yan H (2009) Summary of Northeast Asia geodynamics and tectonics. Stephan Mueller Spec Publ Ser 4:11–33
Passchier CW, Trouw RAJ (1998) Micro-tectonics. Springer, Germany
Petrov OV, Pospelov II, Shokalsky SP (2014) Legend and tectonic zoning of Northern, Central and Eastern Asia (Central Asian fold belt and adjacent tectonic structures) In: Petrov OV, Leonov YG, Pospelov II (eds) Tectonics of Northern, Central and Eastern Asia. Explanatory Note to the Tectonic map of Northern–Central–Eastern Asia and Adjacent Areas at scale 1:2 500 000. – SPb.: VSEGEI Printing House, pp 18–32. http://ccgm.org/en/maps/172-tectonic-map-of-northern-central-and-eastern-asia-9785937612151.html
Pfiffner OA, Ellis S, Beaumont C (2000) Collision tectonics in the Swiss Alps: insight from geodynamic modelling. Tectonics 19:1065–1094
Poblet J, Lisle RJ (2011) Kinematic evolution and structural styles of fold-and-thrust belts. Geol Soc Spec Publ Lond 349:1–24. doi:10.1144/SP349.1
Purevjav N, Roser B (2013) Geochemistry of Silurian–Carboniferous sedimentary rocks of the Ulaanbaatar terrane, Hangay-Hentey belt, central Mongolia: Provenance, paleoweathering, tectonic setting, and relationship with the neighbouring Tsetserleg terrane. Chemie de Erde 73(4):481–493. doi:10.1016/j.chemer.2013.03.003
Purevsuren B, Narantsetseg O (1991) Geological sheet maps M-48-125-D; M-48-137-A, B, C, D; M-48-138-A, B, C, D; L-48-5-A, B at the scale of 1:50 000 with explanatory report. Geological Information Center, Mineral Resource Authority of Mongolia, Ulaanbaatar, Report #4597, pp 10–40
Purevsuren B, Narantsetseg O (1998) Geological sheet maps M-48-105-C, D; M-48-106-C; M-48-117-A, B at the scale of 1:50 000 with explanatory report. Geological Information Center, Mineral Resource Authority of Mongolia, Ulaanbaatar, Report #5157, pp 12–44
Riedel W (1929) Zur Mechanik geologischer Brucherscheinungen. Zentralblatt für Mineralogie Abteilung B:354–368
Roest WR, Srivastava SP (1991) Kinematics of the plate boundaries between Eurasia, Iberia and Africa in the North Atlantic from the late Cretaceous to the present. Geology 19:613–616
Ruppen D, Knaf A, Bussein D, Winkler W, Chimedtseren A, Quadt A (2013) Restoring the Silurian to Carboniferous northern active continental margin of the Mongol-Okhotsk Ocean in Mongolia: Hangay-Hentey accretionary wedge and seamount collision. Gondwana Res 25(4):1517–1534
Ruzhentsev SV, Minina OR, Aristov VA, Katyukha YP (2006) Hercynian structural features in the West Transbaikalia region. Russ J Earth Sci 8:ES2001. doi:10.2205/2006ES000192
Ruzhentsev SV, Aristov VA, Minina OR, Golionko BG, Nekrasov GE (2007) Hercynides of the Ikat-Bagdarin Zone in Transbaikalia. Dokl. Earth Sci 417(8):1198–1201
Ruzhentsev SV, Minina OR, Nekrasov GE, Aristov VA, Golionko BG, Doronina NA, Lykhin DA (2012) The Baikal–Vitim fold system: structure and geodynamic evolution. Geotectonics 46(2):87–110
Ryabinin AB, Buslov MM, Zhimulev FI, Travin AV (2011) The Late Paleozoic fold-thrust structure of the Tunka bald mountains, East Sayan (southern framing of the Siberian Platform). Russ Geol Geophys (Geologiya i Geofizika) 52(12):1605–1623
Schönberg T, Pasotti M (2016) Innstereo Documentation.
Sengör AMC, Natal'in BA (1996) Turkin-type orogeny and its role in the making of the continental crust. Annu Rev Earth Planet Sci 24:263–337
Sengör AMC, Natal'in BA, Burtman VS (1993) Evolution of the Altaid tectonic collage and Paleozoic crustal growth in Eurasia. Nature 364:299–307
Sinclair HD, Gibson M, Naylor M, Morris RG (2005) Asymmetric growth of the Pyrenees revealed through measurement and modeling of orogenic fluxes. Am J Sci 305:369–406
Slejko D, Carulli GB, Nicolich R, Rebez A, Zanferrari A, Cavallin A, Doglioni C, Carraro F, Castaldini D, Iliceto V, Semenza E, Zanolla C (1989) Seismotectonics of the eastern Southern Alps: a review. Bollettino di Geofisica Teorica ed Applicata 31(122):109–136
Stacey JS, Kramers JD (1975) Approximation of terrestrial lead isotope evolution by a 2-stage model. Earth Planet Sci Lett 26(2):207–221
Stagpoole V, Nicol A (2008) Regional structure and kinematic history of a large subduction back thrust: Taranaki Fault, New Zealand. J Geophys Res 113:B01403. doi:10.1029/2007JB005170
Stern TA, Stratford WR, Salmon ML (2006) Subduction evolution and mantle dynamics at a continental margin: Central North Island, New Zealand. Rev Geophys 44:RG4002. doi:10.1029/2005RG000171
Storti F, Salvini F, McClay K (2000) Synchronous and velocity-partitioned thrusting and thrust polarity reversal in experimentally produced, doubly-vergent thrust wedges: Implications for natural orogens. Tectonics 19(2):378–396. doi:10.1029/1998TC001079
Streckeisen AL, Le Bas MJ (1991) The IUGS systemic of igneous rocks. J Geol Soc 148:825–833
Suzuki T, Nakane Y, Bakhat N, Takeuchi M, Tsukada K, Sersmaa G, Khishigsuren S, Manchuk N (2012) Description of sandstones in the Ulaanbaatar area, Mongolia. Bull Nagoya Univ Museum 28:27–38. http://www.num.nagoya-u.ac.jp/outline/report/pdf/028_03.pdf
Takeuchi M, Tsukada K, Suzuki T, Nakane Y, Sersmaa G, Manchuk N, Kondo T, Matsuzawa N, Bakhat N, Khishigsuren S, Onon G, Katsurada Y, Hashimoto M, Yamasaki S, Matsumoto A, Oyu-Erdene B, Bulgantsengel M, Kundyz S, Enkhchimeg L, Ganzorig R, Myagmarsuren G, Jamiyandagva O, Molomjamts M (2012) Stratigraphy and geological structure of the Paleozoic system around Ulaanbaatar, Mongolia. Bull Nagoya Univ Museum 28:1–18. doi:10.18999/bulnum.028.01
Tang J, Xu W, Wang F, Zhao S, Wang W (2016) Early Mesozoic southward subduction history of the Mongol–Okhotsk oceanic plate: Evidence from geochronology and geochemistry of Early Mesozoic intrusive rocks in the Erguna Massif, NE China. Gondwana Res 31:218–240
Tchalenko JS and Ambraseys NN (1970) Structural analysis of the Dash-e-Bayaz (Iran) earthquake fractures. Geol Soc Am Bull 81:41–60
Tolokonnikova Z, Ernst A, Wyse Jackson PN (2014) Palaeobiogeography and diversification of Tournaisian–Viséan bryozoans (lower–middle Mississippian, Carboniferous) from Eurasia. Palaeogeogr Palaeoclimatol Palaeoecol 414:200–211. doi:10.1016/j.palaeo.2014.08.023
Tomur S, Lhavgasuren J, Gerelmaa N (1994) Geological sheet maps M-48-117-C, D; M-48-118-C, M-48-129-A, B, C, D; M-48-130-A at the scale of 1:50 000 with explanatory report.

Geological Information Center, Mineral Resource Authority of Mongolia, Ulaanbaatar, Report #4859, pp 22–81

Tomurtogoo O (2003) Tectonic map of Mongolia at the scale of 1:1 000 000 and tectonics of Mongolia (brief explanatory notes of the map). Mineral Resources Authority of Mongolia, Ulaanbaatar

Tomurtogoo O (2006) Tectonic framework of Mongolia. In: Tomurhuu D, Natal'in BA, Ariunchimeg Y, Khishigsuren S, Erdenesaihan G (eds) Structural and Tectonic Correlation across the Central Asian Orogenic Collage: Implications for Continental Growth and Intracontinental Deformation (second international workshop and field excursions for IGC Project 480), abstract and excursion guidebook. Mongolian University of Science and Technology Press, Ulaanbaatar, pp 18–20

Tomurtogoo O (2012) Tectonic subdivision of Mongolian orogenic belts. Haiguulchin Journal 46:20–35. http://ccgm.org/en/maps/172-tectonic-map-of-northern-central-and-eastern-asia-9785937612151.html

Tomurtogoo O (2014) Tectonics of Mongolia. In: Petrov OV, Leonov YG, Pospelov II (eds) Tectonics of Northern, Central and Eastern Asia. Explanatory Note to the Tectonic map of Northern–Central–Eastern Asia and Adjacent Areas at scale 1:2 500 000. –SPb.: VSEGEI Printing House, pp 110–126

Tomurtogoo O, Byamba J, Badarch G, Minjin Ch, Orolmaa D, Khosbayar P, Chuluun D (1998) Geologic map of Mongolia at the scale of 1:1 000 000 and Summary (explanatory notes of the map). Mineral Resources Authority of Mongolia, Ulaanbaatar

Tovuudorj D (2003) Geological sheet map M-48-XXIX at the scale of 1:200 000 with brief legend description. Geological Information Center, Mineral Resource Authority of Mongolia, Ulaanbaatar, Report #5566, pp 1–66

Tseden Ts, Murao S, Dorjgotov D (1992) Introduction of geology of Mongolia. Bull Geol Surv Jpn 43(12):735–744. https://www.gsj.jp/data/bull-gsj/43-12_01.pdf

Tsukada K, Otoh S, Kurihara T, Bayambadash D, Chuluun M, Gochigdorj S, Nuramkhaan M (2010) Structure of the eastern Khangai-Khentei belt, Mongolia. In: 117th Annual Meeting of the Geological Society of Japan Abstract O-59. doi:10.14863/geosocabst.2010.0.124.0

Tsukada K, Nakane Y, Yamamoto K, Kurihara T, Otoh S, Kashiwagi K, Minjin Ch, Sersmaa G, Manchuk N, Niwa M, Tokiwa T (2013) Geological setting of basaltic rocks in an accretionary complex, Khangai–Khentei belt, Mongolia. Island Arc 22:227–241. https://www.gsj.jp/data/bull-gsj/43-12_01.pdf

Van der Voo R, van Hinsbergen DJJ, Domeier M, Spakman W, Torsvik TH (2015) Latest Jurassic-earliest Cretaceous closure of the Mongol-Okhotsk Ocean: a paleomagnetic and seismological-tomographic analysis. In: Anderson TH, Didenko AN, Johnson CL, Khanchuk AI, MacDonald JH Jr (eds) Late Jurassic Margin of Laurasia—a record of faulting accommodating plate rotation, vol 513. Geological Society of America Special Paper, pp 589–606. doi:10.1130/2015.2513(19)

Wiedenbeck M, Alle P, Corfu F, Griffin WL, Meier M, Oberili F, Quadt AV, Roddick JC, Spiegel W (1995) Three natural zircon standards for U-Th-Pb, Lu-Hf, trace element and REE analyses. Geostand Newslett 19:1–23

Willett S, Beaumont C, Fullsack P (1993) Mechanical model for the tectonics of doubly vergent compressional orogens. Geology 21:371–374

Windley BF, Alexeiev D, Xiao W, Kröner A, Badarch G (2007) Tectonic models for accretion of the Central Asian Orogenic Belt. J Geol Soc Lond 164:31–47

Woodcock NH, Mort K (2008) Classification of fault breccias and related fault rocks. Geol Mag 145(3):435–440. doi:10.1017/S0016756808004883

Xiao W, Windley BF, Hao J, Zhai M (2003) Accretion leading to collision and the Permian Solonker suture, Inner Mongolia, China: termination of the central Asian orogenic belt. Tectonics 22(6):1069. doi:10.1029/2002TC001484

Zhimulev FI, Safonova I, Ryabinin A, Buslov M (2010) An Early Proterozoic metamorphic basement of the Tuva–Mongolia microcontinent as a part of the Tunka fold–nappe terrane (South Siberia): constraints from U/Pb geochronology. EGU General Assembly Conference Abstracts 12, 2285. ftp://ftp.gfz-potsdam.de/home/cegit/egu/pdf/EGU2010-2285.pdf

Zhimulev FI, Buslov MM, Glorie S, De Grave J, Fidler MA, Izmer A (2011) Relationship between the Ordovician and Carboniferous–Permian collisional events in the southeastern Tunka bald mountains, East Sayan (southwestern framing of the Siberian Platform). Russ Geol Geophys 52:1634–1642

Zorin YA (1999) Geodynamics of the western part of the Mongolia-Okhotsk collisional belt, Transbaikal region (Russia) and Mongolia. Tectonophysics 306:33–56